JOURNAL OF GEOPHYSICAL RESEARCH, VOL. 103, NO. B3, PAGES 4839–4878, MARCH 10, 1998

Eurasian surface wave tomography: Group velocities

Michael H. Ritzwoller and Anatoli L. Levshin
Department of Physics and CIRES, University of Colorado, Boulder

Abstract. This paper presents the results of a study of the dispersion characteristics of broadband fundamental surface waves propagating across Eurasia. The study is broader band, displays denser and more uniform data coverage, and demonstrates higher resolution than previous studies of Eurasia performed on this scale. In addition, the estimated group velocity maps reveal the signatures of geological and tectonic features never before displayed in similar surface wave studies. We present group velocity maps from 20 s to 200 s period for Rayleigh waves and from 20 s to 125 s for Love waves. Broadband waveform data from about 600 events from 1988 through 1995 recorded at 83 individual stations across Eurasia have produced about 9000 paths for which individual dispersion curves have been estimated. Dispersion curves from similar paths are clustered to reduce redundancy, to identify outliers for rejection, and to assign uncertainty estimates. On average, measurement uncertainty is about 0.030-0.040 km/s and is not a strong function of frequency. Resolution is estimated from "checker-board" tests, and we show that average resolutions across Eurasia range from 5° to 7.5° but degrade at periods above about 100 s and near the periphery of the maps. The estimated maps produce a variance reduction relative to the Preliminary Reference Earth Model (PREM) of more than 90% for Rayleigh waves below 60 s period but reduce to about 70% between 80 and 200 s period. For Love waves, variance reductions are similar, being above 90% for most periods below 100 s and falling to 70% at 150 s. Synthetic experiments are presented to estimate the biases that theoretical approximations should impart to the group velocity maps, in particular source group time shifts, azimuthal anisotropy, and systematic event mislocations near subducting slabs. The most significant problems are probably caused by azimuthal anisotropy, but above 100 s the effect of source group time shifts may also be appreciable. These effects are probably below the signal levels that we interpret here, however. Many known geological and tectonic structures are observed in the group velocity maps. Of particular note are the signatures of sedimentary basins, continental flood basalts, variations in crustal thickness, backarc spreading, downgoing slabs, and continental roots. Comparison of the estimated group velocity maps with those predicted by CRUST5.1/S16B30 is qualitatively good, but there are significant differences in detail which provide new information that should help to calibrate future crustal and upper mantle models of Eurasia.

1. Introduction

This paper presents the results of a study of the dispersion characteristics of broadband Rayleigh (20-200 s) and Love (20-150 s) waves propagating across Eurasia. These results are presented as group velocity maps which represent the local group velocity of a Rayleigh or a Love wave at each period. There are two main motivations for this study. First, the group velocity maps that result from this study provide new constraints on the shear velocity structure of the crust and uppermost mantle underlying Eurasia. These maps display better resolution and should be more reliable (lower variance and bias) than globally estimated dispersion maps or such maps computed from current global models of the crust and mantle. They should also help to calibrate future generations of global dispersion maps and seismic models and to provide valuable, transportable data to be used in future inversions for the shear velocity structure of Eurasia. Second, accurate high-resolution group velocity maps are useful in monitoring clandestine nuclear tests. These maps guide the identification and extraction of surface waveforms which emanate from small seismic events. The estimation of surface wave magnitude, M_s, is thereby facilitated for use as part of, for example, the $M_s : m_b$ method of discriminating under-

Paper number 97JB02622.
0148-0227/98/97JB-02622$09.00

ground explosions from naturally occurring earthquakes [e.g.,*Stevens and Day*, 1985].

The study of surface wave dispersion was begun independently by *Love* [1911] and *Golitzin* [1912]. Surface wave dispersion studies applied to understanding the structure of the Earth date from the 1920s and 1930s with the early works or *Gutenberg* [1924, 1926], *Jeffreys* [1928, 1935], *Stoneley* [1926, 1928], *Byerly* [1930], *Gutenberg and Richter* [1936], and others. The "modern era" of surface wave dispersion research probably began with the studies of *Press* [1956] and *Press et al.* [1956] and was ushered in by the text of *Ewing et al.* [1957]. The flurry of surface wave studies that took place in late 1950s and continued throughout the 1960s defined "classical dispersion analysis" but is too voluminous to list. However, *Ewing et al.* [1957] presents a review that is relatively complete into the late 1950s, and subsequent reviews were presented by *Oliver* [1962], *Dziewonski* [1971], and *Knopoff* [1972, 1983]. In the 1980s, surface waveform fitting became popular and *Nolet* [1987] and *Snieder* [1993] present reviews. However, classical dispersion studies based on both single-station and multistation or multievent methods continue in common practice today. Most current dispersion studies are little different from those in the 1960s other than that computers are far faster, seismic instrumentation has been vastly improved, and there is now much more complete path coverage across most regions of interest. Together, these improvements allow tomographic methods to be applied to very large numbers of surface wave dispersion measurements to produce broadband maps of surface wave dispersion over wide areas.

We present the results of a classical single-station dispersion study and the subsequent estimation of dispersion maps using standard tomographic methods. The study is distinguished by its broadbandedness, the relatively high resolution of the resulting group velocity maps, and its geographical scale. We present surface wave maps across Eurasia between 20 s and 200 s period. Measurements are regularly obtained down to 10 s and up to 250 s period, but the reliability of the group velocity maps across large regions of the continent degrades sharply below 20 s and above about 150-200 s for Rayleigh waves and 100-125 s for Love waves. Surface wave maps at and below 30 s period are particularly important since they provide significant constraints on crustal thickness by helping to resolve Moho depth from the average shear velocity of the crust [e.g., *Das and Nolet*, 1995]. Although there have been numerous studies of surface wave dispersion that have produced measurements of group and/or phase velocities between 10 and 40 s period, these studies have typically been confined to areas of about 15° or less in lateral extent. We are not aware of any study to date that has provided detailed dispersion maps below 30 s period over an area as large as Eurasia. We argue below that we determine the sign and approximate location of group velocity features between 5° and 7.5° in spatial extent at most periods across most of the continent.

The scale of this study is somewhat unusual in surface wave studies. Most surface wave studies are performed either regionally (average path lengths $\Delta < 1500$ km) or globally ($\Delta > 10{,}000$ km). There have been a very large number of regional surface wave studies in Eurasia. Some of these from last 20 years, segregated coarsely by geographical region, include those in the following lists. In Europe there are the largest number of studies, they include *Nolet* [1977], *Calcagnile and Panza* [1978, 1979, 1980, 1990], *Mueller and Sprecher* [1978], *Calcagnile et al.* [1979, 1985], *Levshin and Berteussen* [1979], *Panza et al.* [1978, 1980], *Neuenhofer et al.* [1981], *Mantovani et al.* [1985], *Snieder* [1988], *Mindevalli and Mitchell* [1989], *Dost* [1990], *Yanovskaya et al.* [1990], *Stange and Friederich* [1993], *Vaccari and Panza* [1993], *Pedersen et al.* [1994], and *Lomax and Snieder* [1995]. In the Middle East, central Asia, and China there are the studies of *Chen and Molnar* [1975], *Knopoff and Fouda* [1975], *Bird and Toksoz* [1977], *Chun and Yoshii* [1977], *Pines et al.* [1980], *Knopoff and Chang* [1981], *Wier* [1982], *Romanowicz* [1982], *Feng et al.* [1983], *Jobert et al.* [1985], *Brandon and Romanowicz* [1986], *Lyon-Caen* [1986], *Bourjot and Romanowicz* [1992], *Levshin et al.* [1992], *Wu and Levshin* [1994], *Levshin et al.* [1994], *Levshin and Ritzwoller* [1995], *Ritzwoller et al.* [1996b], *Zhang* [1997], *Wu et al.* [1997], A. Curtis and J. Woodhouse (Crust and upper mantle shear structure beneath the Tibetan Plateau and surrounding regions from inter-event surface wave phase velocity inversion, submitted to *Geophysical Journal International*, 1996), and D.A. Griot et al. (Surface wave phase velocity tomography and azimuthal anisotropy in central Asia, submitted to *Journal of Geophysical Research*, 1997, hereinafter referred to as Griot et al., submitted manuscript, 1997). In northern Asia, surface wave studies are fewer in number but include *Lander et al.* [1985], *Kozhevnikov and Barmin* [1989], *Zeng et al.* [1989], and *Kozhevnikov et al.* [1992]. Dispersion studies performed on a global scale usually are based on waveform fitting. Some of the more recent of these include the studies of *Zhang and Tanimoto* [1993], *Su et al.* [1994], *Laske* [1995], *Trampert and Woodhouse* [1995, 1996], *Laske and Masters* [1996], *Li and Romanowicz* [1996], *Masters et al.* [1996], and *Ekström et al.* [1997]. A review is given by *Ritzwoller and Lavely* [1995].

The present study is on a continental-scale, performed at a length-scale intermediate between regional and global surface wave studies. The improvements in resolution and bandwidth over global-scale studies result from the mixture of measurements obtained from surface waves which propagate both regionally (Δ <3000 km) and continent-wide (Δ >6000 km). Regionally propagating surface waves provide many of the measurements at the short-period end of the spectrum and improve resolution appreciably. Their use alone, however, would provide rather patchy path coverage, would result in very strong sensitivity to errors caused by event mislocation and azimuthal anisotropy, and would not yield many measurements at periods longer than about 60 s. Utilizing measurements from both the regional and continental scales allows us to combine the best characteristics of regional and global studies and provides a data set that is strongly and differen-

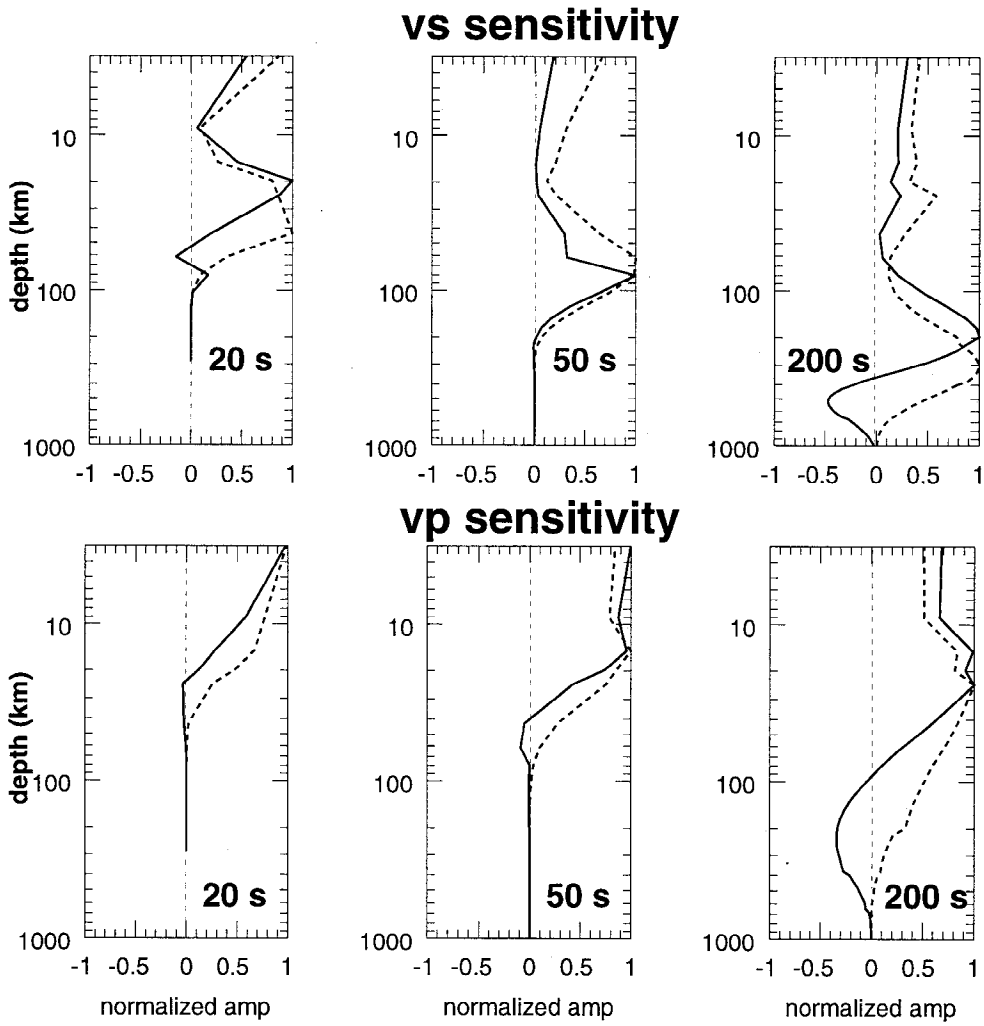

Figure 1. Rayleigh wave phase (dashed lines) velocity and group (solid lines) velocity sensitivity kernels to shear velocity and compressional velocity at three periods computed for PREM.

tially sensitive to both crustal and upper mantle structures. Other studies of Eurasia on a continental scale include those of *Patton* [1980], *Feng and Teng* [1983a], *Lerner-Lam and Jordan* [1983], *Levshin et al.* [1996], and A. Curtis and R. Snieder (Surface wave phase velocities and shear velocity structure beneath Eurasia, manuscript in preparation, 1997). There are, however, advantages to the regional- and global-scale studies. Resolution can be locally better in the regional studies, especially those based on multistation or multievent methods, and global studies are generally more reliable at long periods at and beyond about 150 s for Rayleigh waves and 125 s for Love waves.

Another aspect of this study which is perhaps somewhat unusual is that it is a group velocity rather than a phase velocity study. We have performed a group velocity study for three reasons. First, measurements of group velocities are much less sensitive to source effects than phase velocities [e.g., *Knopoff and Schwab*, 1968; *Muyzert and Snieder*, 1996] since they derive from measurements of the wave packet envelopes rather than the constituent phases. This is particularly true at shorter periods and longer ranges. This has allowed us to use small events for which no moment tensor has been estimated. Second, as Figure 1 shows, group velocity sensitivity kernels are compressed nearer to the surface than the related phase velocity kernels, which should provide further help in resolving crustal from mantle structures. Finally, it is group velocity rather than phase velocity that is needed to extract surface waveforms for seismic discrimination. It should be noted that the group velocity maps that are presented here are intrinsically different from group velocity maps derived from the frequency derivative of phase velocity maps or approximate relationships between phase and group velocity. As described in section 2, the group velocities estimated in this study involve measurements made on the group envelope rather than the phases that constitute the envelope. Hence the group velocities presented here place constraints on the velocity structure of Eurasia independent of phase information. We will present the phase velocity maps that are estimated from the phases that constitute the wave packet envelope in a future contribution.

Although some recent surface wave studies have produced phase velocity maps that possess azimuthal aniso-

tropy [e.g., *Tanimoto and Anderson*, 1985; *Nishimura and Forsyth*, 1988; *Montagner and Tanimoto*, 1990, 1991; *Trampert and Woodhouse*, 1996; Griot et al., submitted manuscript, 1997], our maps do not demonstrate this feature. However, our maps do display polarization anisotropy (transverse isotropy, horizontal fast axis). Polarization anisotropy is expressed as a specific differential perturbation to the Rayleigh and Love wave velocities at each spatial point [*Montagner and Nataf*, 1986]. In general, relative to the best fitting isotropic model, polarization anisotropy manifests itself by speeding up the Love wave and slowing down the Rayleigh wave. The estimated maps presented here contain this information and therefore should not be seen as isotropic but rather as transversely isotropic. In many locations, no realistic isotropic model can be found that will simultaneously fit both the Rayleigh and Love waves, especially at periods above about 100 s.

There are several key assumptions or approximations on which this study rests. We assume that the effects of the following phenomena on the estimated group velocity maps are small compared to the size of the heterogeneity interpreted in each map and that their accumulated impact does not greatly change the character of the estimated maps either quantitatively or qualitatively: (1) the deviation of ray paths from the great-circles linking the sources to the receivers, (2) azimuthal anisotropy, (3) mislocations of earthquake epicenters, and (4) source group time shifts. We refer to errors in these assumptions generically as "theoretical errors." The effects of the last three of these theoretical errors on the estimated group velocity maps are estimated quantitatively and discussed in section 4.2. The first phenomenon, the effect of ray path deviation from great circles, is discussed only qualitatively.

The outline of the paper is as follows. Section 2 presents a discussion of the data used in the study and the method of measurement used to produce the estimated group velocity curves. Section 3 discusses the tomographic method used to translate the measured group velocity curves into group velocity maps as each period and for each wave type (Rayleigh or Love). Section 4 presents a discussion of uncertainties expected in the estimated group velocity maps. This discussion breaks into two parts. Section 4.1 discusses uncertainties not related to theoretical errors which result mainly from the distribution of wave paths in number and azimuth and from data weighting and damping in the inversion. These types of uncertainties are summarized in an analysis of resolution and bias. Section 4.2 presents a discussion of uncertainties that result directly from theoretical errors. A sampling of the estimated group velocity maps is presented in section 5 and the maps are discussed in section 6. In particular, the discussion concentrates on identifying the types of geological and tectonic features in the crust and uppermost mantle that are distinguishable in the estimated group velocity maps. It is these features that will be constrained by the use of the estimated group velocity maps in inversions for the shear velocity structure of the crust and upper mantle under Eurasia, such as the study of *Ritzwoller et al.* [1996a]. The estimated maps are compared with group velocity maps predicted from the hybrid model composed of the crustal model CRUST5.1 of *Mooney et al.* [1997] together with the mantle model S16B30 [*Masters et al.*, 1996].

2. Data and Measurement

Eurasia is an ideal site to perform surface wave tomography. Broadband station coverage has been very good across most of the continent for several years, Eurasia is nearly surrounded by nearby plate boundaries, and it is the continent that possesses the most significant intracontinental seismicity (Figure 2). Thus surface wave path density and azimuthal distribution over much of the continent are good and many relatively short paths (<4000 km) are available for analysis, at least below about 40 s period. These factors in combination control resolution and bias, as discussed in section 3.

The goal of the measurement phase of this research is to obtain accurate estimates of surface wave characteristics (group and phase velocity, amplitude, and polarization in some cases) for each source-receiver pair and to estimate the uncertainty in these measurements. The most significant issues that must be addressed include the accrual of high-quality waveform data, the identification and extraction of unwanted signals, the measurement of the dispersion characteristics of the signals of interest, the rejection of bad measurements, and the estimation of measurement uncertainties.

Data quality from both global (e.g., Global Digital Seismic Network (GDSN), Global Seismic Network (GSN), Geoscope) and regional (e.g., Chinese Digital Seismic Network (CDSN), Kyrghyz Seismic Network (KNET), Kazakhstan Seismic Network (KAZNET), Mediterranean Seismic Network (MEDNET)) networks is very good. The main problem to be faced is that Eurasia is structurally complicated. This not only makes interpretation in terms of structural models difficult, it also complicates the identification of the aspects of the waveforms on which measurement methods should be applied. Our aim is to extract the nearly directly arriving surface waves that can be interpreted simply and deterministically from the potentially interfering multipaths and coda, which are more complicated and stochastic in nature.

The basic characteristics of the current measurement procedure are based on a long history of the development of surface wave analysis [e.g., *Dziewonski et al.*, 1969; *Landisman et al.*, 1969; *Levshin et al.*, 1972, 1989, 1992, 1994; *Cara*, 1973; *Herrin and Goforth*, 1977; *Feng and Teng*, 1983b; *Russell et al.*, 1988; *Ritzwoller et al.*, 1995] and are described in detail by *Levshin et al.* [1992], which refers to the method as frequency-time analysis (FTAN). FTAN is exemplified in Figure 3. Group velocity versus period diagrams for the vertical, radial, and transverse components are constructed and graphically displayed. An analyst manually traces the apparent group velocity curve for the Rayleigh wave (on the vertical and radial components) and the Love wave

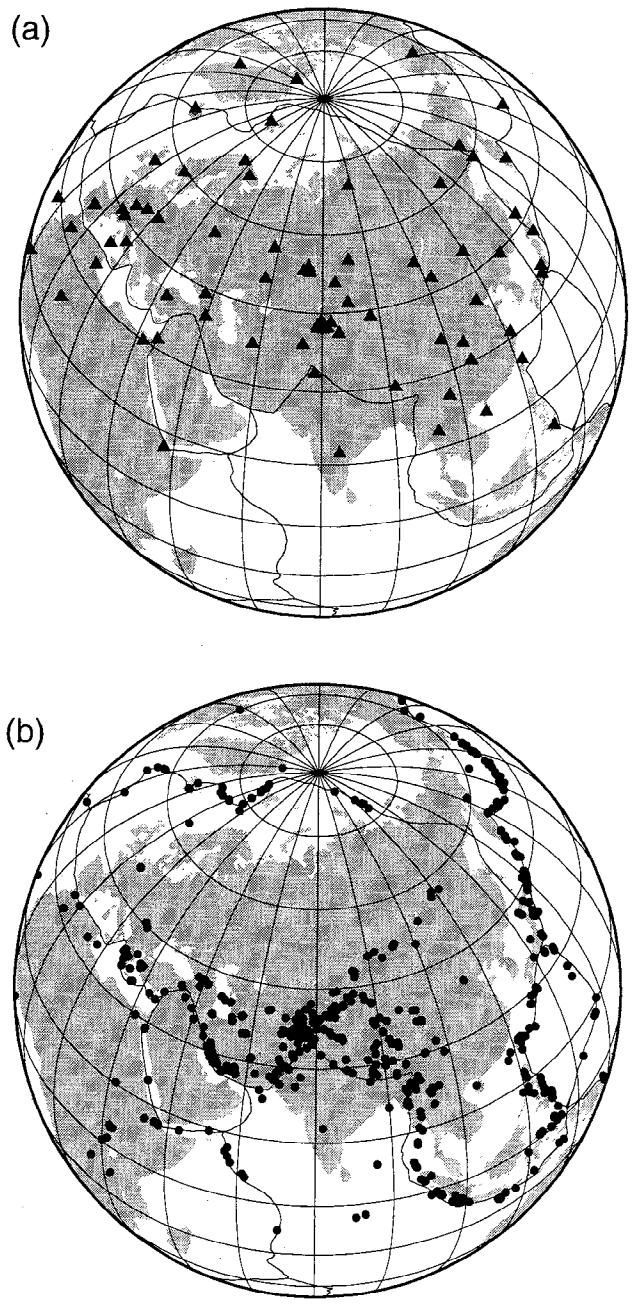

Figure 2. Locations of (a) stations (triangles) and (b) events (circles) used in this study.

(on the transverse component) to define time-variable filters which are applied around the selected curve in order to separate the desired signal from the "noise"; in particular, surface wave coda, overtones, and body waves. This results in filtered group velocity versus period diagrams on which contamination from interfering signals should be reduced. Group time, phase time, amplitude, and polarization measurements are automatically obtained on the filtered images. Group velocity and phase velocity are computed from the distance between the receiver and the centroid moment tensor (CMT) location [*Dziewonski et al.*, 1981] when it exists, and the preliminary determination of epicenters (PDE) location otherwise. The analyst tailors the bandwidth of each measurement to the individual seismogram and assigns a qualitative grade to each measurement (A-F).

The success of this method depends on the analyst accurately identifying the fundamental dispersion ridge, separating the "direct arrival" from surface wave coda at periods below about 30 s, inspecting interpolation near spectral holes, and truncating the measurements appropriately at short and long periods as the signals weaken. This interaction limits the speed of the method, and therefore the volume of data that can be processed. However, it is necessary to insure that the measurements possess the desired quality, especially at the short- and long-period ends. The method has been streamlined sufficiently to allow rapid progress to be made.

To date, we have applied FTAN to waveform data from approximately 600 events in and around Eurasia which occurred from the beginning of 1988 through mid-1995 (Figure 2). Waveforms from most of the events which took place around Eurasia during this time period with $M_s \geq 5.0$ were acquired and processed. However, in regions of particularly high seismic activity (e.g., Kurile Islands region, Taiwan, Honshu, Philippines) a higher magnitude threshold of at least $M_s = 5.5$ was used. Particular attention was devoted to optimizing resolution in central Asia, and we processed events with M_s as low as 4.0 that occurred in this region subsequent to the installation of KNET in late 1991. Waveform data were obtained from seven networks (CDSN, GDSN, Geoscope [*Romanowicz et al.*, 1984], GSN, KAZNET [*Kim et al.*, 1995], KNET [*Pavlis et al.*, 1994; *Vernon*, 1994], MEDNET) comprising 83 individual broadband stations. The application of FTAN to these waveform data has yielded more than 9000 measured Rayleigh wave dispersion curves and more than 7600 Love wave dispersion curves. The total number of curves as a function of period and wave type (Rayleigh/Love) is shown in bold in Figure 4.

By design, the resulting data set exhibits considerable redundancy, which allows for consistency tests, outlier rejection, and estimation of measurement uncertainties. These tests are performed as part of what we call a "cluster analysis". Measurements whose path endpoints lie within 2% of the path length are grouped to produce a "cluster" of dispersion curves. This cluster defines a "unique path." Frequently, these clusters are composed of a large earthquake and its aftershocks recorded at a single station, but in some cases, nearby stations (e.g., stations in KNET and KAZNET; MAJO/INU) allow clustering from a single earthquake. All dispersion curves that are not part of some cluster individually define a unique path.

An example of a cluster of dispersion curves is shown in Figure 5a for a set of five events in the Philippines recorded at Eskdalemuir, Scotland (ESK). Outliers are identified in two ways. First, a measurement is accepted only if it falls within a fairly broad group velocity corridor. Second, measurements that form part of a cluster are compared and visually inspected if there is significant disagreement. An analyst then interactively chooses which measurements to discard, if

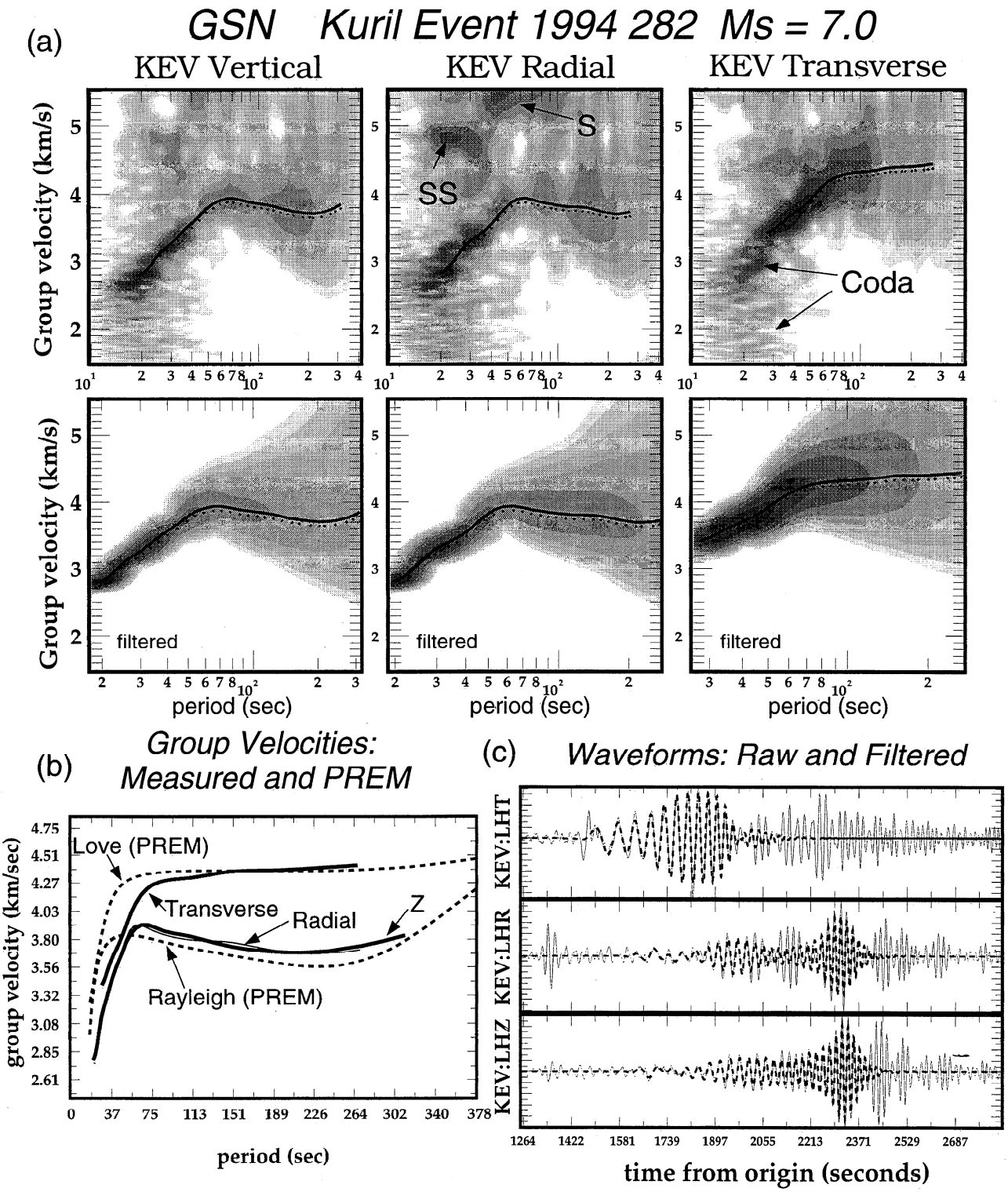

Figure 3. FTAN. Example of a frequency-time analysis for the vertical, radial, and transverse components recorded at the GSN station at Kevo, Finland for an event in the Kurile Islands (October 9, 1994, M_s = 7.0, Δ = 58.5°). (a) The analyst-defined filter removes potentially interfering signals such as body waves, other surface waves, overtones, and coda. Group velocity curves are estimated automatically on the filtered images. (b) Rayleigh and Love wave group velocity measurements (solid lines) are compared with the predictions from PREM (dashed lines). (c) Comparison of the raw (thin solid) with the filtered (bold dashed) waveforms reveals the effect of the filtering displayed in Figure 3a.

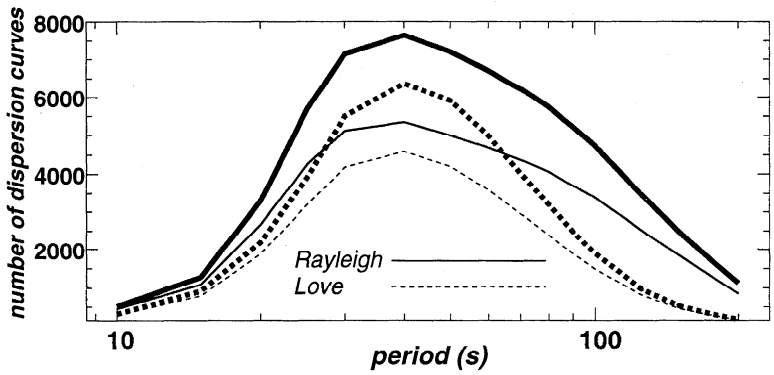

Figure 4. The number of dispersion measurements before (bold lines) and after (thin lines) the cluster analysis. Rayleigh waves are solid lines, and Love waves are dotted lines.

any. Higher-graded measurements from larger events are given precedence in the selection process. After outlier rejection, the average velocity and standard deviation of the cluster are assigned to the path. The number of clusters as a function of period is shown in Figure 5b, and the number of unique paths is displayed in Figure 4 as the thin lines. About one-third of the original dispersion curves at intermediate periods are part of some cluster. The average path length as a function of period is presented in Figure 5c. The standard deviation of the dispersion curves within each cluster averaged over all clusters is plotted as a function of period and wave type in Figure 5d. We interpret this standard deviation as the average measurement uncertainty which we then associate with all dispersion curves that are not part of a cluster. Thus, if a dispersion curve has resulted from a cluster of measured curves, the uncertainty attributed to that curve arises from the variation among the individual curves composing the cluster. If the curve is for a ray that is not part of a cluster, the average of the standard deviations of the measurements taken over all clusters is used to define the measurement uncertainty.

The estimates of measurement uncertainty presented in Figure 5d are estimates of repeatability. The effects of some systematic theoretical errors, such as those caused by event mislocations, azimuthal anisotropy, or lateral ray refractions and scattering, may not be incorporated in these estimates. The effects of theoretical errors on the estimated group velocity maps will be discussed in section 4.2.

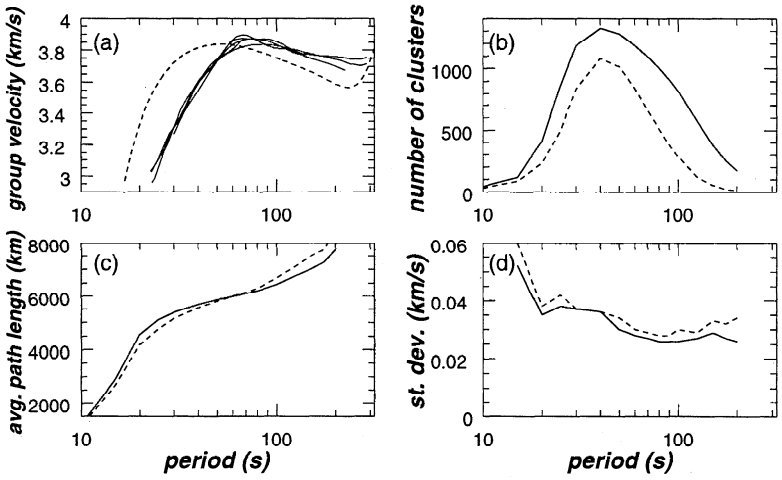

Figure 5. Cluster analysis. (a) Example of a cluster of measured group velocity curves. Estimated Rayleigh wave group velocity curves from a set of five events in the Philippines measured at Eskdalemuir (ESK), Scotland, are compared with one another (solid lines) and the group velocity curve predicted from PREM (dashed line). (1989, 349, $M_s = 7.4$; 1990, 39, $M_s = 6.6$; 1991, 49, $M_s = 6.6$; 1991, 317, $M_s = 6.4$; 1992, 138, $M_s = 7.1$). (b) The total number of clusters in the data set plotted as a function of period and wave type (Rayleigh, solid line; Love, dashed line.) (c) The average path length versus period (Rayleigh, solid; Love, dashed). (d) The average of the standard deviation of the group velocity curves composing all of the clusters. These values are assigned as uncertainties to all measured group velocity curves which are not part of some cluster.

3. Surface Wave Tomography

This paper presents the first part of an inversion for crustal and uppermost mantle structure beneath Eurasia. This inversion is broken into two stages: (1) the estimation of broadband group velocity maps at a variety of periods for both Rayleigh and Love waves and (2) the inversion of these maps for a shear velocity model. We call the estimation of group velocity maps "surface wave tomography" and this first stage of the inversion is as far as this paper extends. We describe the nature of surface wave tomography in this section and present a sampling of the estimated group velocity maps in the subsequent sections of the paper. The second stage of the inversion has begun [e.g., *Ritzwoller et al.*, 1996a] and will be reported elsewhere.

We employ the algorithm of *Ditmar and Yanovskaya* [1987] and *Yanovskaya and Ditmar* [1990] to construct the group velocity maps [see also *Levshin et al.*, 1989; Chapter 6] using the group velocity curves that emerge from the cluster analysis applied to measurements made with the frequency-time analysis (FTAN). The method of Yanovskaya and Ditmar is a generalization to two dimensions of the classical one dimensional method of *Backus and Gilbert* [1968, 1970]. There are several features that commend this method. First, it does not require any a priori parameterization or truncation of any expansion since the basis functions for the model are superpositions of the kernels of the group travel time integrals. Perhaps more importantly, the method has been well tested and provides a well-understood foundation for our work. The major disadvantages of the method, as we use it, are that it does not include explicit penalties on model size or the second spatial derivative of the model and the ray basis functions lead to artifacts caused by bad measurements. Thus outliers must be identified and rejected a priori and the maps must be smoothed in a rational manner a posteriori.

For each frequency and wave type, group velocity is a local function of position, $U(\theta,\phi)$, which we decompose into some reference value (frequently, the average across the studied region), U_0, and a location dependent perturbation, $U(\theta,\phi) = U_0 + \delta U(\theta,\phi)$. The most significant characteristics of this method are as follows. (1) The method seeks a smooth perturbation in group velocity, $\delta U(\theta,\phi)$, relative to a homogeneous model, U_0, such that $U(\theta,\phi)$ fits the N observed group velocity travel times, $t_i^{\rm obs} (i = 1,..,N)$, in a weighted least squares sense. To do this, the method attempts to minimize the following penalty function at each period and wave type:

$$\sum_{i=1}^{N} [w_i (t_i^{\rm obs} - t_i^{\rm pred})]^2 + \lambda \int_S |\nabla U(\theta,\phi)|^2 dA, \qquad (1)$$

where

$$t_i^{\rm pred} = \int_{p_i} U^{-1}(\theta,\phi) ds. \qquad (2)$$

Here p_i represents the ith wave path, w_i is the weight associated with the ith path through the group velocity map $U(\theta,\phi)$, $t_i^{\rm pred}$ is the predicted group travel time along the ith path, and S is the region under study. Choosing different values of the trade-off parameter, λ, changes the trade-off between the fit to the data and the "smoothness" of the resulting group velocity map. "Smooth" here is defined in terms of the first spatial gradient of the model. The inversion takes place independently for each period and wave type. (2) Relative group velocity variations are assumed to be small in amplitude for each period and wave type: $\delta U(\theta,\phi)/U_0 << 1$. This is the justification for a linearized inversion procedure. (3) In equation (2), we currently assume that each wave path is along the great circle linking the source and receiver and no group time perturbation is introduced by a source phase shift.

Data weights result from three subweights. The weight for measurement i is

$$w_i = \sqrt{m} \frac{g_i}{\sigma_i}, \qquad (3)$$

where m is the number of raw measurements that compose the cluster that produced this measurement, σ_i is the uncertainty determined from the cluster analysis for measurement i, and g_i is a weight which depends on the qualitative grade (A-F) assigned to the measurement by the analyst. As discussed in section 2, if a measurement has resulted from a cluster, the uncertainty, σ_i, is the standard deviation of the dispersion curves composing the cluster. If a measurement has not resulted from a cluster, the average of the standard deviations from all clusters is taken as the uncertainty. The weight g_i is defined as follows. The normative grade is A and receives a weight of 1.0. Grades of B, C, D, E, and F are given weights of 0.75, 0.4, 0.2, 0.0, and 0.0, respectively. Thus no measurement receiving a grade less than D is used. The grades of the measurements composing a cluster are averaged to produce a cluster grade which is then subjected to the same weighting criteria. For ungraded measurements, $g_i = 0.5$.

The damping parameter λ in equation (1) is chosen subjectively by analyzing misfit, the visual smoothness, and the physical reasonableness of the resulting group velocity maps. Figure 6 illustrates the trade-off curve between misfit and λ for the 40 s Rayleigh wave. Misfit is presented, first, as variance reduction relative to the average value across a given map

$$\text{variance reduction} = 1 - \frac{\sum_i (U_i^{\rm obs} - U_i^{\rm pred}(\lambda))^2}{\sum_i (U_i^{\rm obs} - U_0)^2}, \qquad (4)$$

where i is the unique path index, $U_i^{\rm pred}(\lambda)$ is the predicted group velocity for path i through the group velocity map constructed with the damping parameter set to λ, $U_i^{\rm obs}$ is the measured group velocity for path i, and U_0 is the reference group velocity. In Figure 6, U_0 is the average group velocity across the map. Misfit is also presented as the rms velocity residual

$$\text{rms misfit} = \left(\frac{1}{N} \sum_{i=1}^{N} (U_i^{\rm obs} - U_i^{\rm pred}(\lambda))^2 \right)^{1/2}. \qquad (5)$$

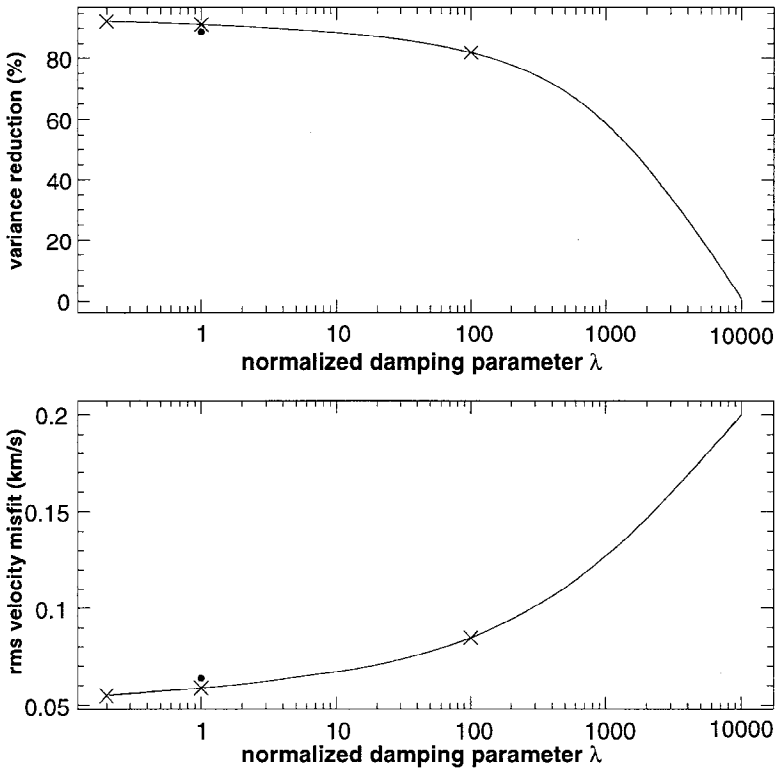

Figure 6. Two measures of misfit as a function of the damping parameter λ in equation (1) for the 40 s Rayleigh wave. The damping parameter has been normalized such that its value is unity for the slightly underdamped case. Three values of the normalized damping parameter are indicated as crosses on the trade-off curves: one severely underdamped ($\lambda \sim 0.2$), one slightly underdamped ($\lambda \sim 1$), and one highly overdamped ($\lambda \sim 100$). The group velocity maps constructed with these three values of λ are shown in Plate 1. The application of the a posteriori smoothing filter (full width at e^{-1} point is 2.5°) to the group velocity map from the slightly underdamped inversion degrades fit to the data by a small amount, as is indicated by the closed circle. (top) Variance reduction relative to the average group velocity across the slightly underdamped map. (bottom) Rms velocity difference between the observed group velocities and those predicted from the group velocity maps.

Three points on the misfit curves are marked with a cross: one overdamped, one slightly underdamped, and one severely underdamped. Determination of whether a map is overdamped or underdamped is almost purely subjective. A map is termed overdamped if physically reasonable features are missing from it that appear in maps with less damping. Clearly underdamped maps display aphysical speckling, streaking, and other artifacts. The rms misfit and variance reduction are, unfortunately, not good indicators of the "quality" of a map, in particular they are not very useful in determining the appropriate damping. In particular, these overall measures of misfit are changed minimally by small-scale features. They are therefore poor indicators of the reliability of the estimated small scale anomalies. Thus, although the slightly underdamped map ($\lambda \sim 1$, variance reduction ~90%) produces a much better fit to many individual dispersion curves for paths through small-scale features than the highly overdamped map ($\lambda \sim 100$), the total variance reduction is only marginally improved from 85%.

Group velocity maps for each of the dampings in Figure 6 are shown in Plate 1. We typically choose λ to produce a slightly underdamped map. Because the penalty function does not include a spatial second derivative term, we smooth each map a posteriori by applying a Gaussian spatial-smoothing filter with a carefully chosen width. The width chosen depends both on wave type and period and derives from the resolution analyses discussed in section 4. This smoothing is designed to be an antialiasing filter, and we apply it such that the full width at e^{-1} of the maximum height of the filter is half the estimated average resolution for the map. For example, for a 40 s Rayleigh wave the Gaussian filter's full width is 2.5° at the e^{-1} point. The effect of this filter is also shown in Plate 1 as the "smoothed" map. A posteriori smoothing reduces artifacts, minimally degrades overall fit to the data (Figure 6), retains most of the physically reasonable small-scale features, and improves coherence between maps with similar periods.

4. Uncertainties in the Estimated Group Velocity Maps: Resolution and Bias

Uncertainties in the estimated group velocity maps result from several sources of two general types. The

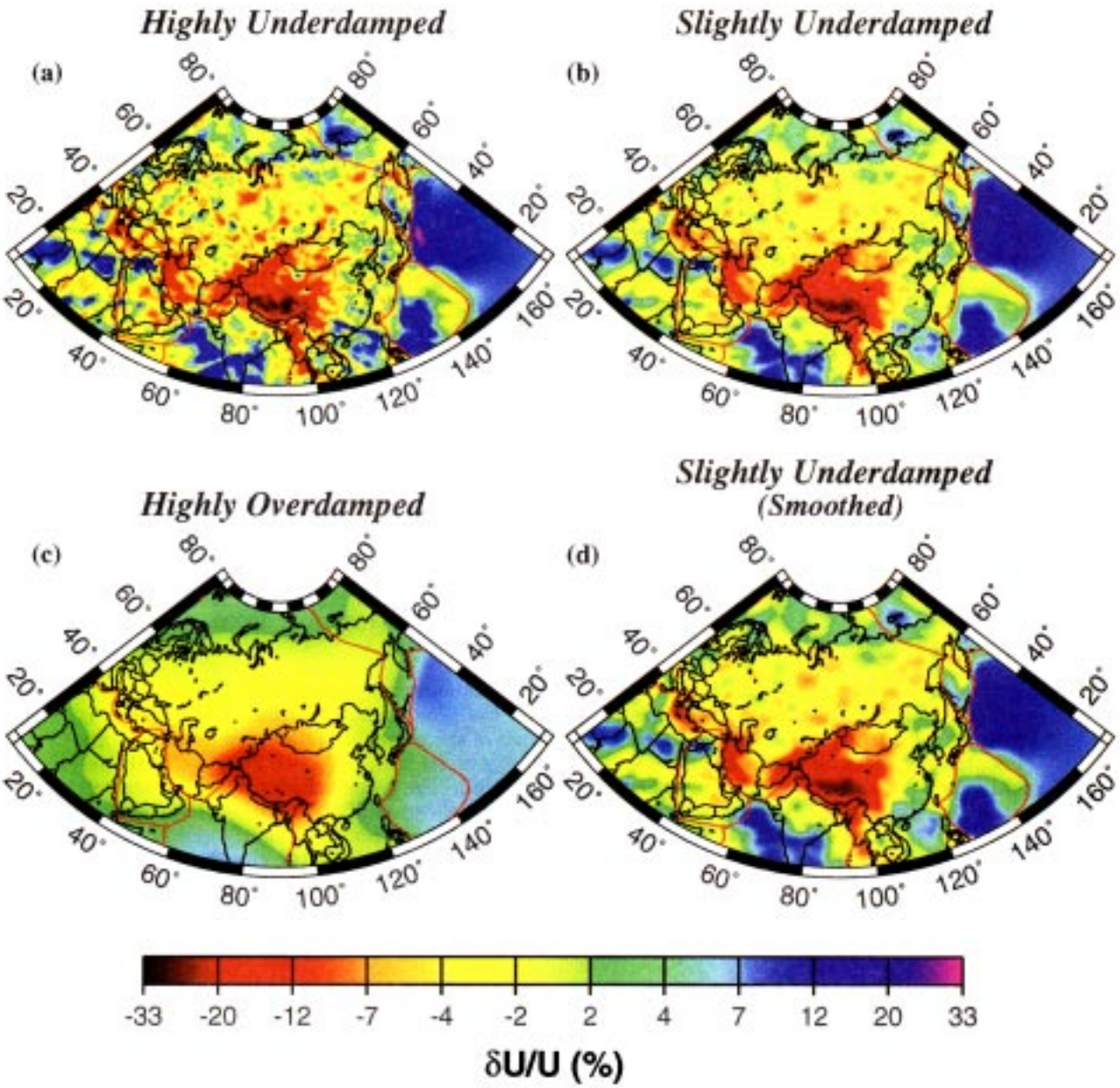

Plate 1. Group velocity maps constructed with the three damping parameters that are indicated with crosses in Figure 6: (a) highly underdamped ($\lambda \sim 0.2$), (b) slightly underdamped ($\lambda \sim 1$), and (c) highly overdamped ($\lambda \sim 100$). (d) Map produced by applying the a posteriori smoothing filter (full width at the e^{-1} point of 2.5°) to the map in Plate 1b.

first type of uncertainty results from measurement errors and the vagaries of path distribution. Of these, the more severe are the effects of path distribution. At a chosen level of damping in the inversion, path distribution, both density of wave paths and azimuthal distribution, controls resolution. In section 4.1 we perform a set of classical checker-board tests to estimate the resolution of and bias in the estimated group velocity maps. As discussed in section 3, these estimates of resolution are used in the construction of a posteriori smoothing filters which are applied to each of the estimated group velocity maps. The second type of uncertainty involves errors in assumptions, approximations, and input parameters which are not estimated in the inversion. Together we refer to these as theoretical errors. The principal theoretical errors that will negatively affect the estimated group velocity maps include event mislocations, azimuthal anisotropy, wave path refractions from the great circle linking source and receiver, and source group time shifts. A discussion of the effects of these issues is the subject of section 4.2. The estimates of both types of uncertainties need to be kept

in mind when interpreting the group velocity maps presented in section 5. This interpretation is the subject of section 6.

4.1. Uncertainties Unrelated to Theoretical Errors

Ignoring theoretical errors, at each geographical point and period the resolution of the data set discussed in section 2 will depend on the density of unique paths, the azimuthal distribution of these paths, their average path length, and the data weighting and damping applied in the inversion. Examples of the path coverage are shown in Figures 7a and 7b where we plot the path density, defined as the number of paths that intersect each square 2° cell (~50,000 km^2). The path density across much of Eurasia is high but falls off rapidly near the periphery of the continent, particularly in India, in North Africa, and in the oceanic regions other than the marginal seas of the western Pacific and much of the Philippine Sea. Path density is highest, particularly at periods below about 60 s, in central Asia due to the presence of KNET and KAZNET. The importance of azimuthal distribution and path length to resolution and bias will be discussed briefly later in this section.

To estimate resolution, we perform a checker-board test. Figure 8a (left) displays three checker-board in-

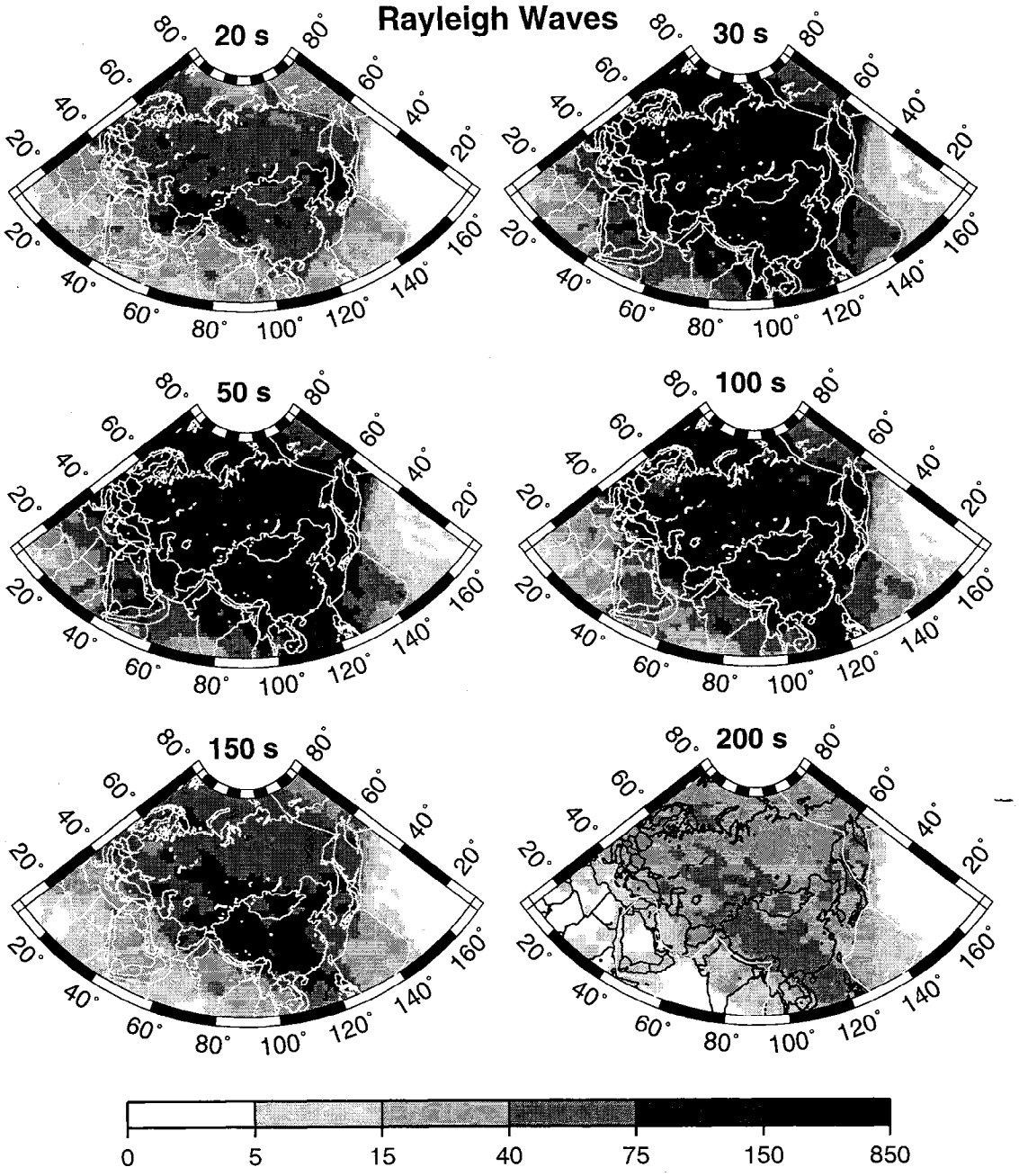

Figure 7a. Path density for Rayleigh waves at the six indicated periods. Path density is defined as the number of rays intersecting a 2° square cell (~ 5×10^4 km^2).

put models. Each model is divided into cells of equal area, where each cell possesses a velocity perturbation of ±10% of the average across each map. Travel time perturbations are accumulated along great circle paths linking source and receiver. Since no noise is added to the synthetic travel times, the estimated resolution is largely independent of the amplitude of the velocity perturbation chosen (±10%). The number and distribution of unique paths differ with period and wave type. We can estimate resolution as a function of wave type and period by computing synthetic travel times through the checker-board model for exactly the unique paths that have emerged from the cluster analysis and then inverting these synthetic data using the same weighting and damping used in the group velocity tomography described in section 3 and applied to real data in section 5.

The estimated maps are displayed in Figure 8a (right). The paths used in Figure 8 are those for the 40 s Rayleigh wave and the cell sizes are 3°, 5°, and 7.5°. (Note that the cells are square. A cell size of n degrees means that the cell is about $n \times 111$ km in both latitude and longitude.) Although a few regions appear to be resolved at 3°, most cells are not resolved until they are increased in size to 5°. When cells are increased in size to 7.5°, nearly all of the cells that can be resolved by the data set are resolved. The regions which possess very poor path coverage in Figure 7, such as those

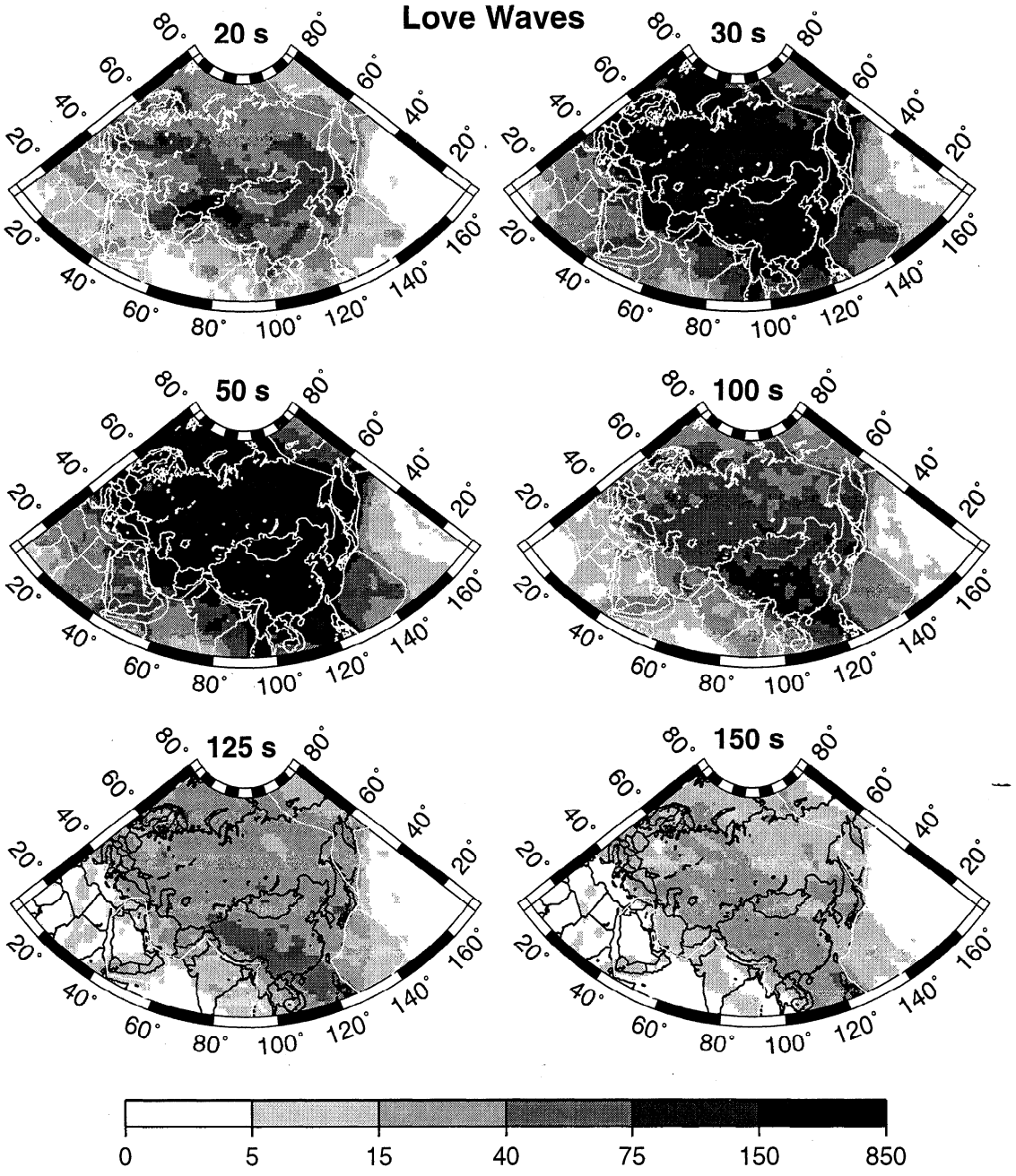

Figure 7b. Same as Figure 7a, but for Love waves at the indicated periods.

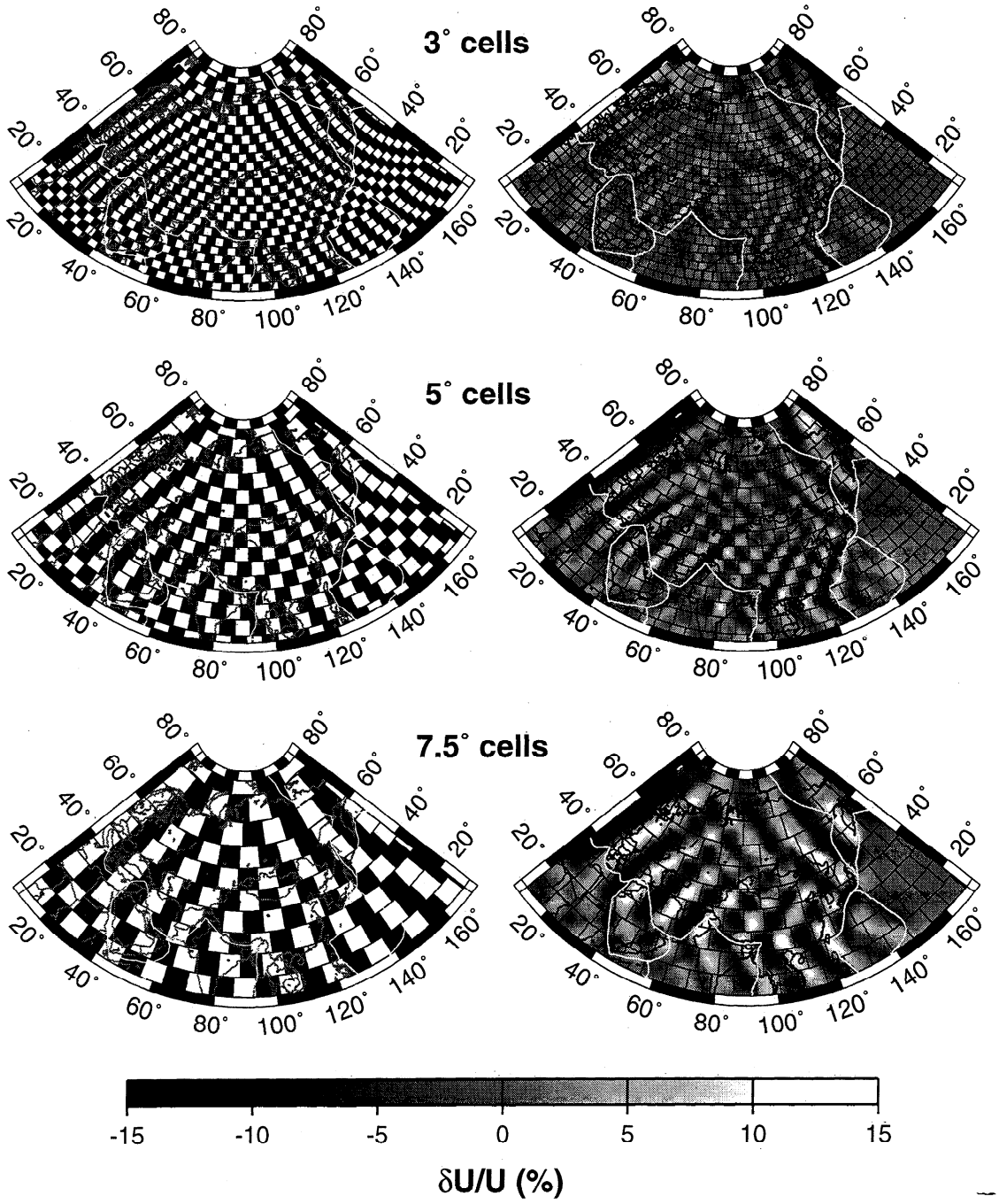

Figure 8a. Checker-board test for the 40 s Rayleigh wave with cells of three different sizes: (top) 3°, (middle) 5°, (bottom) 7.5°. There are regions in which 3° cells are resolved, but if cells are smaller than 5° most are not well resolved. Resolutions of 5° are observed across most of Eurasia, with the notable exception of north central Siberia, where cells are not resolved below about 7.5° in size.

around the periphery of the continent, not surprisingly, display very poor resolutions.

Plots such as those in Figure 8a are rather difficult to interpret and digest in large numbers. The key question is whether or not a given cell has been resolved in the inversion. What is desired principally is a yes or no answer. To simplify interpretation, we assign a 'resolution index', $\mathcal{R}_i$, to each cell:

$$\mathcal{R}_i = \frac{v_{\max}}{v_{\text{input}}} \quad \text{(in percent)}. \tag{6}$$

Here $v_{\max}$ is the estimated velocity deviation whose absolute value is maximum in the cell and v_{input} is the input velocity deviation in the same cell. Perfect resolution for a given cell size would result in $\mathcal{R}_i = 100\%$; poor resolution results in $\mathcal{R}_i \leq 30\%$. The resolution in-

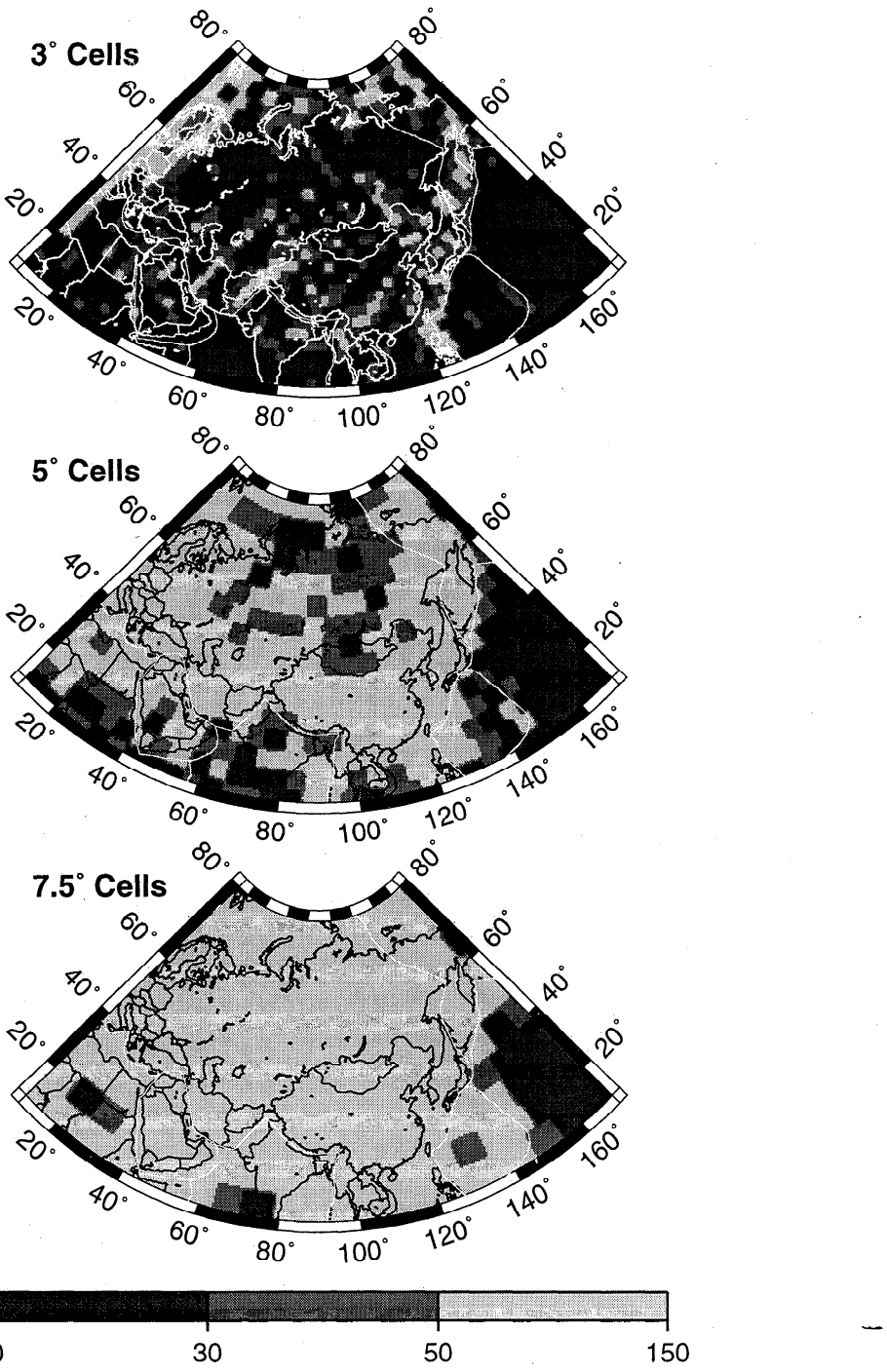

Figure 8b. Plots of the resolution index ($\mathcal{R}_i$, equation (6)) for the 40 s Rayleigh wave with the same cell sizes as in Figure 8a. Light grey cells are considered resolved, increasingly darker cells denote poorer resolution. Units are percent of the input value in each cell.

dex can be less than zero if the sign of $v_{\max}$ is opposite from the input value, v_{input}, of the cell or greater than 100% if the estimated magnitude is higher than the input value. In Figure 8b, we plot the resolution index for each of the three checker-boards in Figure 8a, again with the unique paths for the 40 s Rayleigh wave. Each cell is assigned one of three shades of grey depending on if the cell is considered to be resolved. If $\mathcal{R}_i > 50\%$ the cell is shaded light grey and is considered resolved. The regions with poorer resolutions are indicated by the darker cells. The 50% criterion may seem overly liberal, but we are interested mainly in determining if a feature of a given size is observable rather than determining if we estimate its amplitude correctly. Although these are interesting separate issues, the first spatial derivative damping penalizes both model amplitude and roughness simultaneously. Since we cannot separate these effects during inversion, we must be careful to discrim-

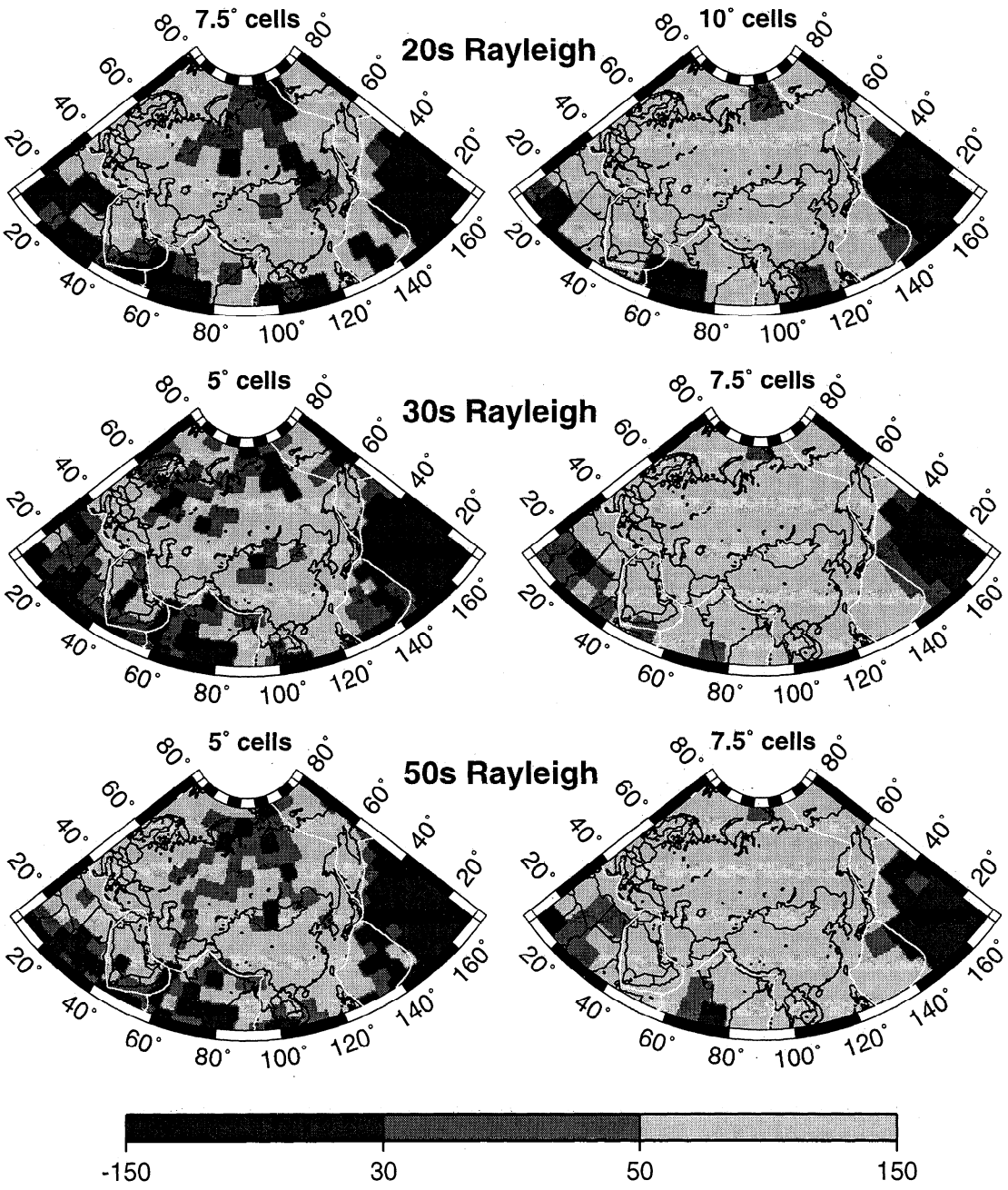

Figure 9a. Resolution index ($\mathcal{R}_i$, equation (6)) plotted for intermediate-period Rayleigh waves at the indicated periods and with the specified cell sizes. Three grey-scale values are presented; the lightest indicates good resolution and increasingly dark cells reveal poorer resolutions. Units are percent of the input value in each cell.

inate between them after the inversion. The relatively liberal criterion of 50% is designed to help do this. (In the future, it may be preferable to attempt to consider spatial and amplitude resolutions separately.) The average resolution emerges as about 5° for a 40 s Rayleigh wave across most of Eurasia, although much of central Siberia is not resolved at 5°.

Figures 9a-9d present a set of maps of the resolution index for both Rayleigh and Love waves at a variety of periods. The tests differ from one another in the cell sizes presented, the number and distribution of the paths that characterize the data set at each period and wave type, and the damping applied during inversion. Each row of these figures presents two resolution index maps, one in which most of Eurasia is resolved but some regions are not quite resolved and the other in which Eurasia is nearly fully resolved. The cell sizes defining these two figures differ from period to period and between wave types. However, a recurring problem emerges: northern and central Siberia tend to be the most poorly resolved regions of Eurasia independent of period and wave type. Figure 10 presents a summary

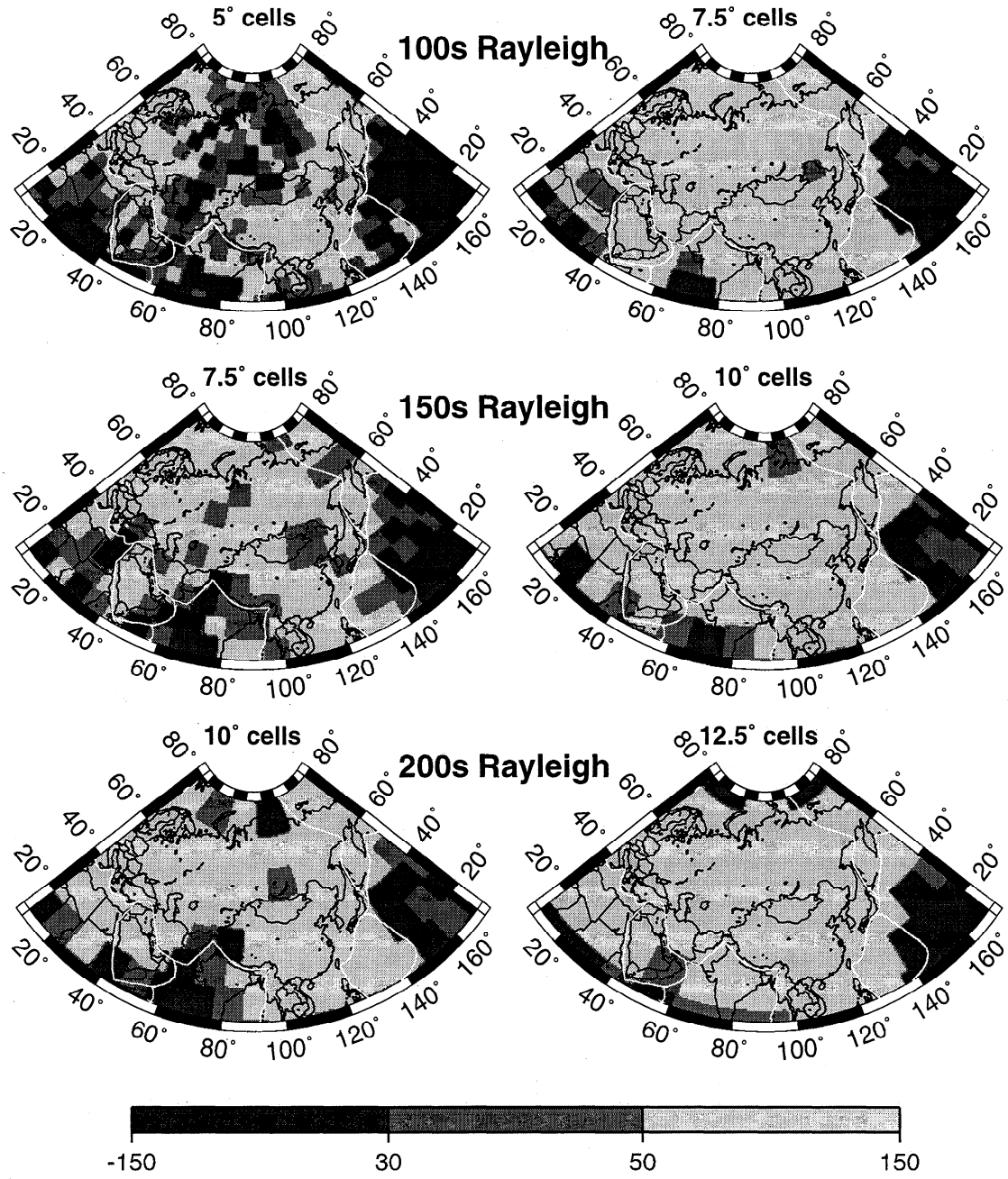

Figure 9b. Same as Figure 9a, but for the long period Rayleigh waves at the indicated periods.

of the minimum cell size for which most of Eurasia is resolved at each period. *Lévêque et al.* [1993] introduce a note of caution concerning the interpretation of analyses such as these. Checker-board test are not fault-free means of estimating resolution.

To estimate bias we perform similar experiments in which only a small number of well spaced cells have nonzero velocities. For example, Figure 11 displays a resolution analysis in which the input model comprises two square 7.5° cells with nonzero structural values (10%), one in a well-resolved region of central Asia and the other in a poorly resolved area of north central Siberia. The rest of the model outside of these blocks is everywhere zero. The ray paths used, again, are the unique paths for the 40 s Rayleigh wave. In the checker-board test, we estimated a resolution of about 5° in central Asia and 7.5° in north central Siberia. Consistent with this test, the estimated central Asian cell is well resolved and unshifted. The Siberian cell, however, is spread out and shifted to the south by about one-half of a cell size. This half-cell bias is below the 5° resolution we report for the 40 s Rayleigh wave in Figure 10. It should be remembered, however, that errors in the estimated group velocity maps may include shifting due to the vagaries of path distribution at a significant fraction of the reported resolution in some regions.

The bias and degraded resolution characterizing north central Siberia are not due to a shortage of ray paths

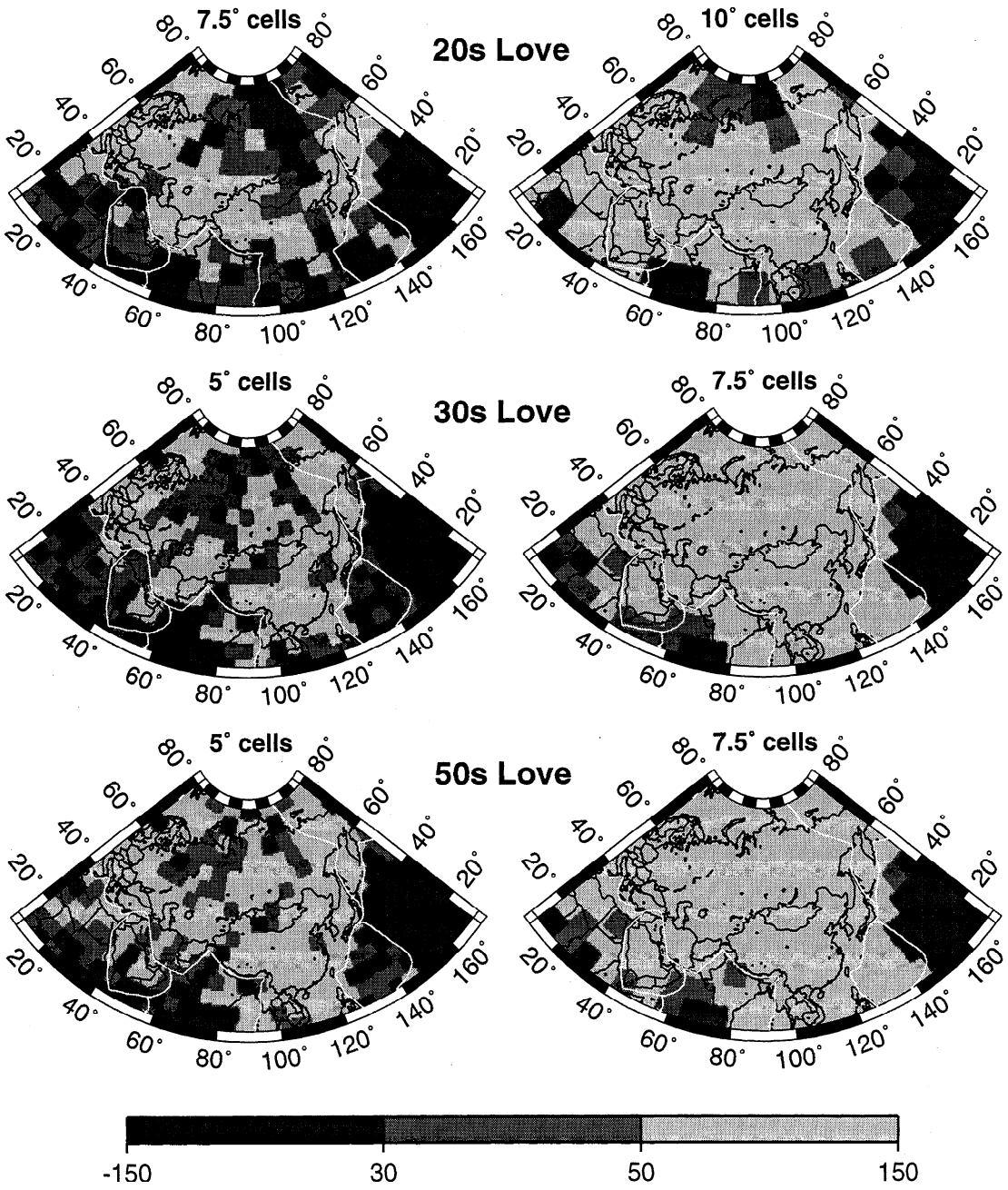

Figure 9c. Same as Figure 9a, but for intermediate period Love waves at the indicated periods.

in this area, as Figure 7a demonstrates. Path density throughout this region is high, although certainly not as high as in central Asia. Furthermore, the azimuthal distribution of paths piercing the central Asian and Siberian cells is about the same. Both regions display a shortage of nearly meridional paths. What differs between these two regions is the existence of large numbers of relatively short paths in central Asia. These short paths allow relatively small cells to be resolved even without a homogeneous azimuthal distribution. However, in the absence of regional seismicity and good seismic station coverage in north central Siberia, the shortage of nearly north-south paths manifests itself as a degradation in resolution. The future addition of more nearly north-south paths originating from events in central Asia and propagating to Canadian National and U.S. National Network stations would help improve resolution throughout much of northern Eurasia.

4.2. Uncertainties Caused by Theoretical Errors

Other sources of bias can result from theoretical errors. We discuss the following here: off-great-circle propagation, event mislocation, source group time shifts, and azimuthal anisotropy. We deal with the first of these issues only qualitatively. The last three error sources we deal with quantitatively by performing syn-

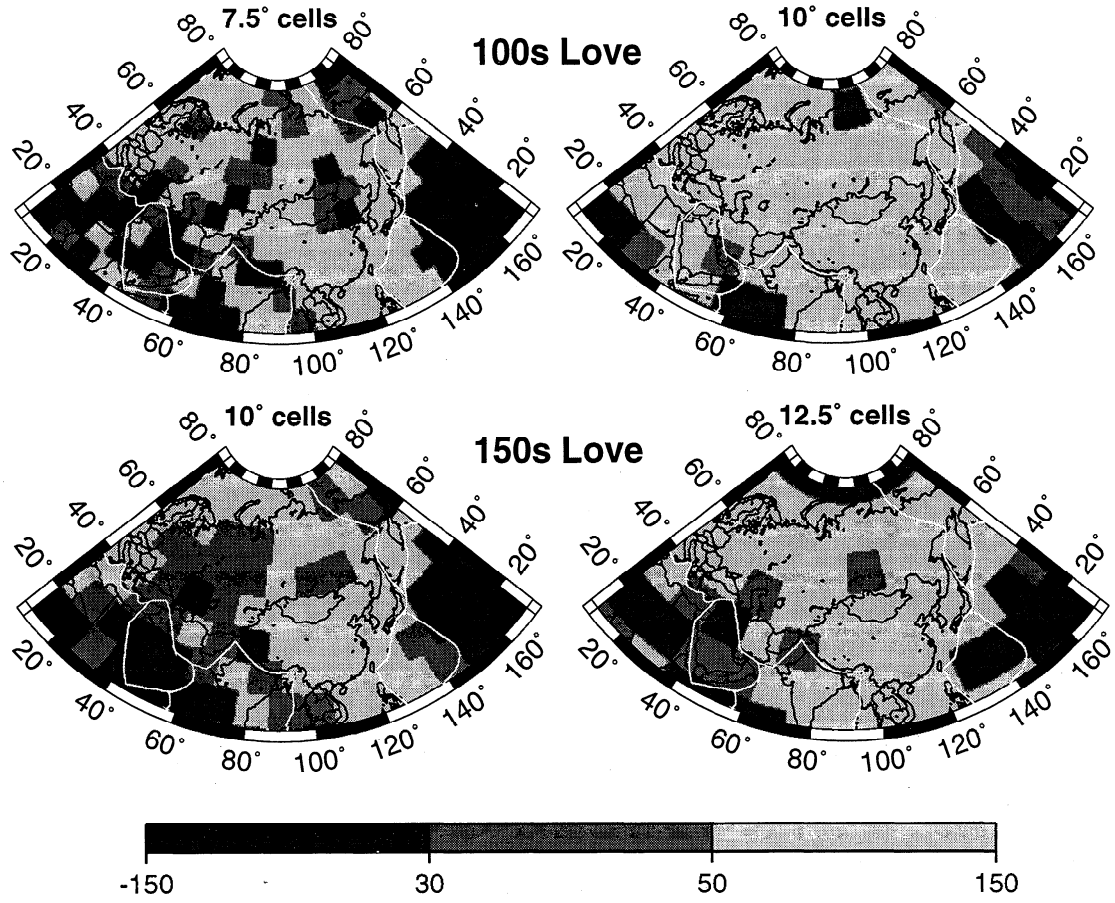

Figure 9d. Same as Figure 9a, but for the long period Love waves at the indicated periods.

thetic tomographic inversions which aim to estimate the effects of each error on the estimated group velocity maps. In each case, we attempt to simulate the effect of the errors on travel times and then invert the erroneous theoretical travel times exactly as the real data are inverted at each period and wave type (same paths, damping, data weighting, a posteriori smoothing, etc.). Naturally, the utility of these experiments will depend on how well we have simulated the error process in each case.

4.2.1. Off-great-circle propagation. A comparison between the locations of known structural boundaries and features apparent in the group velocity maps indicates that tomographic features may be shifted by as much as 3° to 5° in geologically complicated regions, such as much of central Asia. These shifts typically lie below the resolutions that we report here. Part of the shifts may be due to off-great-circle propagation. However, as discussed in section 4.1, part may also be due to path distribution. Thus errors in the estimated

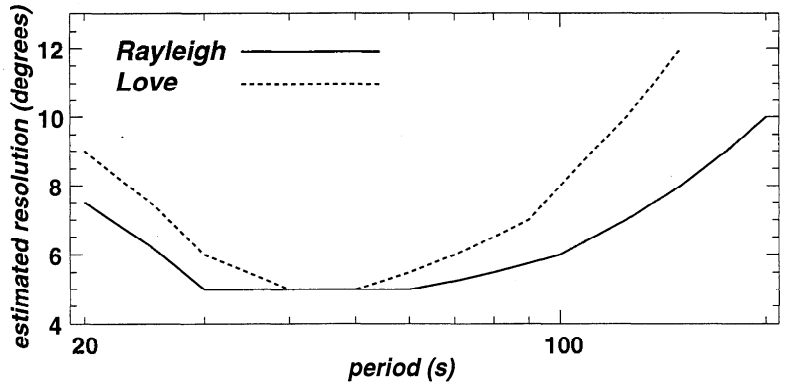

Figure 10. Estimated average resolution across the Eurasian continent. The value of resolution is chosen such that most of the continent appears to be resolved in resolution index plots, such as those shown in Figure 9.

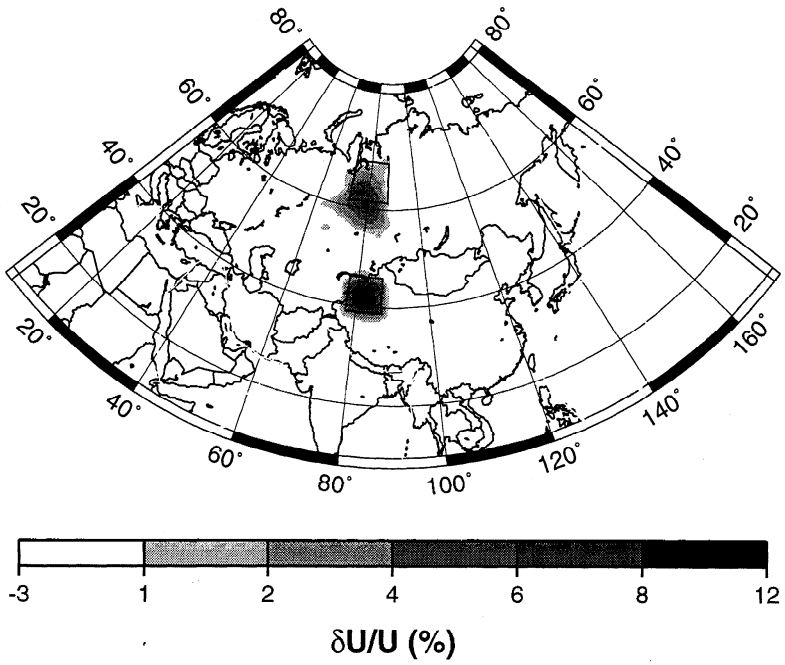

Figure 11. Bias analysis in which there are only two nonzero 7.5° square input cells, one in central Asia (a region of very good resolution) and one in north central Siberia (a region with poor resolution). Synthetic data used are the same as in Plate 1 for the 40 s Rayleigh wave. The input locations and shapes of the cells are shown. Both input cells have a velocity variation of 10%. The rest of the continent is homogeneous with no velocity variation. The estimated tomographic map demonstrates the southern shift of the north central Siberian cell (by about one-half the cell width) and the high fidelity of the estimated central Asian cell.

group velocity maps may include shifting due to off-great-circle propagation at a significant fraction of the reported resolution level in some regions. A more careful simulation of the effects of off-great-circle propagation will be the subject of future research.

4.2.2. Systematic event mislocations. The multiplicity of sources helps mitigate against bias caused by source mislocation. Synthetic experiments show that if mislocations are random, their effect on the estimated group velocity maps is negligible. However, mislocations in certain source regions, in particular those adjacent to subducting slabs, may be systematic. Systematic errors in epicenter estimates of 10 km or more in extended regions may have an appreciable effect on the estimated group velocity maps.

Figure 12 presents examples from a synthetic experiment in which the locations of about 15 events in the Kurile Islands and in the Hindu Kush are shifted systematically and exactly in parallel by 10 km. Mislocations of the events in the these regions may be larger than this, but the fact that all events are shifted in parallel maximizes the effect of the mislocations on the estimated group velocity maps. We shifted the "true", locations of the Kurile events to the southeast and the Hindu Kush events to the south relative to the erroneous locations used in the inversion. Figure 12 presents the tomographic simulation for the 20 s, 50 s, and 150 s Rayleigh waves for the mislocated Kurile events and for the 20 s Rayleigh wave for the mislocated Hindu Kush events. In each inversion, only the events located in the specified regions are shifted; all other event locations are assumed to be known perfectly. Input structure is laterally homogeneous, so that the only "signal" in the synthetic data comes from the event mislocations in the specified region.

The travel time signal due to a 10 km shift is less than 4 s. If a 3-s signal were distributed evenly along a 6000 km path, the resulting velocity perturbation would be only about 0.2% of the average group velocity. However, as Figure 12 shows, in a tomographic inversion the effect of event mislocations is very small outside of the source region and the erroneous signal is compressed into a small region which amplifies the bias. The amplitude of the bias is approximately independent of period, with an absolute value maximizing between 0.5-0.8% of the average group velocity at each period. The size of this bias scales directly with the length of the mislocation. In source regions away from the margins of the continent, such as the Hindu Kush, there are many paths crossing the region which do not originate in the source region. This diminishes the size of the bias. Figure 12 shows that the bias caused by the 10-km perturbation to the Hindu Kush events is less than half that caused by similar perturbations to the locations of the Kurile events.

4.2.3. Source group time shifts. We have assumed that the initial phase imparted by the earthquake only minimally affects group travel time [*Knopoff and Schwab*, 1968]. Figure 13a presents estimates of the expected Rayleigh wave group time shifts for the earth-

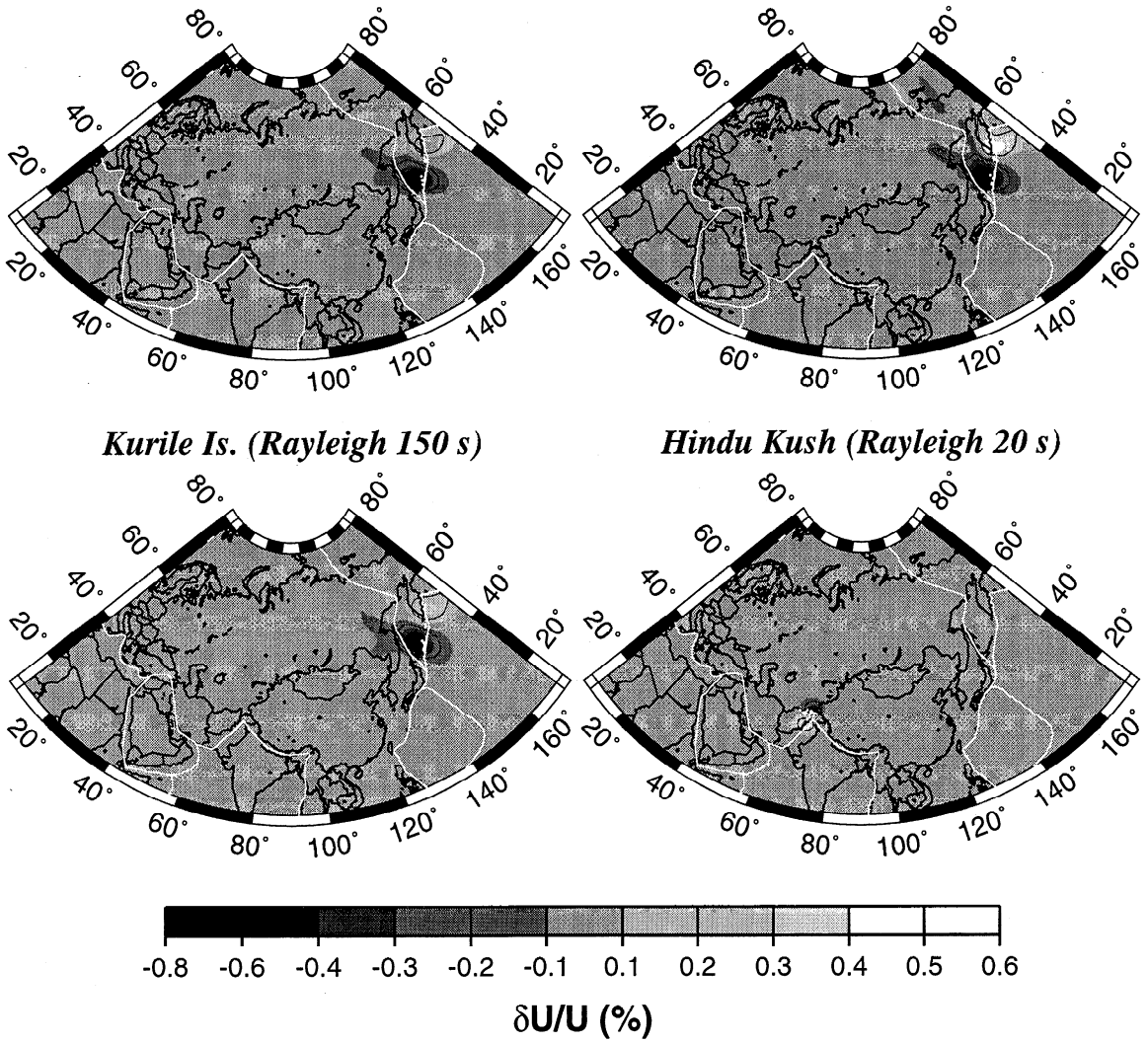

Figure 12. Mislocation bias. Results of a synthetic experiment in which approximately 15 events in two source regions (the Kurile Islands and the Hindu Kush) are shifted in the same direction by 10 km to determine the effect of systematic errors in source locations on the tomographic images. All events in the Kuriles are mislocated to the northwest and in the Hindu Kush to the north. Three Rayleigh wave periods (20 s, 50 s, 150 s) are shown for the Kurile Islands events and one period (20 s) is shown for the Hindu Kush events. Bias is displayed in percent deviation from the average group velocity across the map. Event locations are marked by small white dots. The 0.2% contours are drawn.

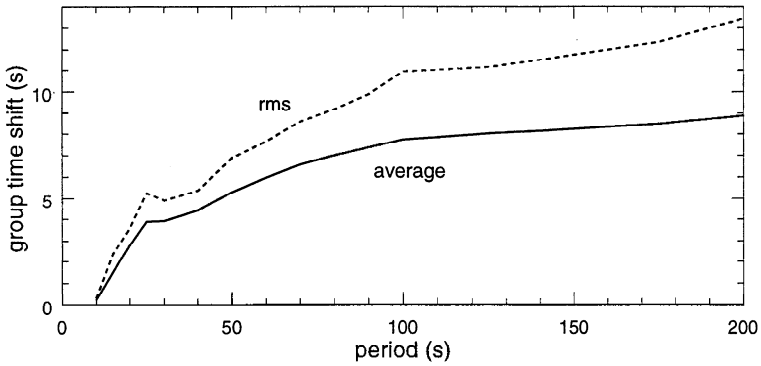

Figure 13a. Estimated expected value of Rayleigh wave group time shifts as a function of period. The median over azimuth of the absolute value of the group time shift is computed for each earthquake. The average and rms of these medians, taken over all of the earthquakes, are plotted here. Group time shifts are computed using the Harvard CMT catalogue for all events for which the CMT solution exists.

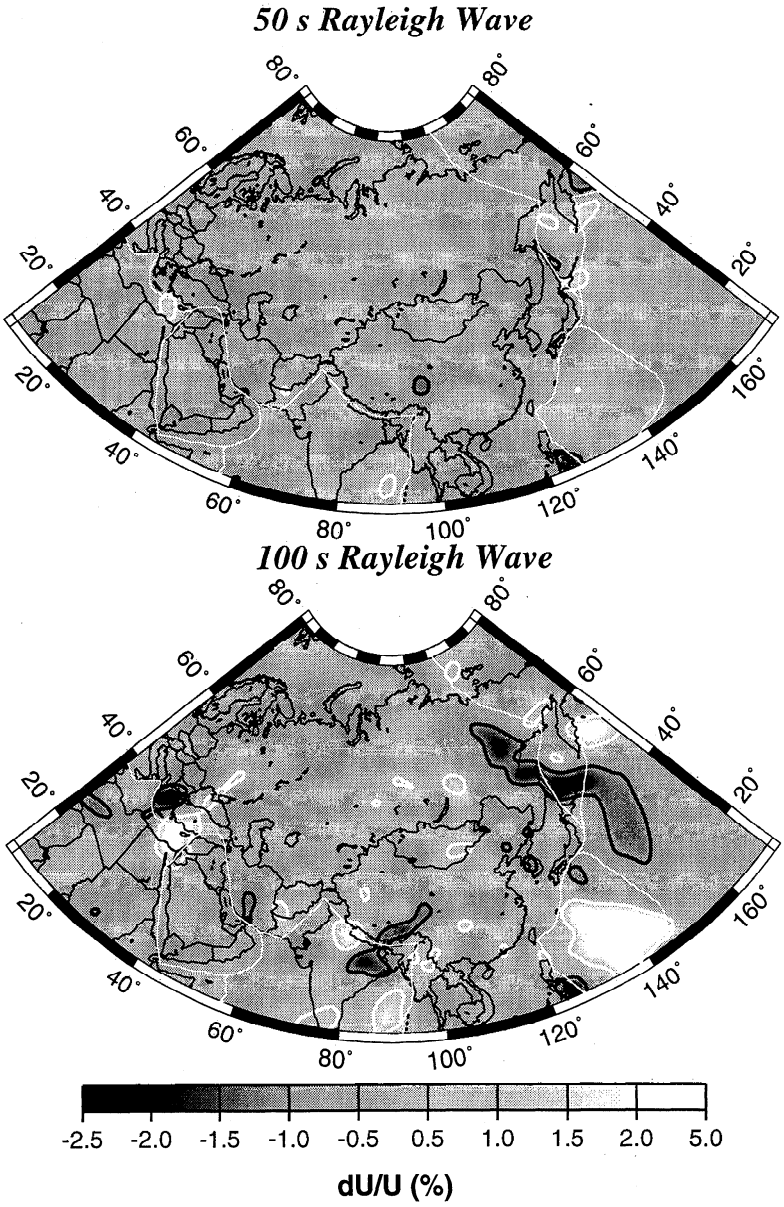

Figure 13b. Source group time shift bias. Estimated bias for the 50 s and 100 s Rayleigh waves caused by source group time shifts, expressed as percent error relative to the average group velocity across the region of study for each period. The ±1% contours are drawn.

quakes used in this experiment. For each earthquake, we used the CMT moment tensor to compute the source group time shift as a function of azimuth. Since this shift amplifies greatly near nodes in the radiation pattern, the average of the absolute values and the rms with azimuth do not provide good estimates of the characteristic amplitude of the group time shift for the event. The median of the absolute values with azimuth provides a better characterization of the event and Figure 13a presents the rms and the average of these medians taken over all of the events in our data set with a CMT solution. The expected group time shifts increase with period and range between about 3-4 s on the short period end of our study to closer to 10 s at long periods. Individual group time shifts may be considerably larger than this, but this normally occurs only near nodes in the radiation pattern where few measurements are actually made.

If focal mechanisms vary spatially in a random manner, time shifts of 5-10 s would produce little bias in the estimated group velocity maps. However, focal mechanisms across large areas are not random, and like source mislocation bias, the bias in the estimated group velocity maps caused by source group time shifts can concentrate in source regions with similar focal mechanisms. Using a synthetic experiment similar to the inversion to estimate the effect of source mislocations, Figure 13b presents estimates of the bias in the 50 s and 100 s Rayleigh wave maps caused by ignoring the group time shift produced by the CMT solution. For the same reasons as for source mislocation, the bias maximizes in source regions near the edge of the continent. Although

the patterns of bias differ somewhat with period, the amplitude of bias is about the same as that shown in Figure 13b at all periods above about 50 s. Thus, we expect that this effect is probably several times the size of errors caused by source mislocations.

4.2.4. Azimuthal anisotropy. The estimated group velocity maps are directionally independent and therefore contain no information about azimuthal anisotropy. The maps are azimuthal averages of group velocity at every point, but since the azimuthal distribution of rays at every point across each map is not uniform, it is a legitimate concern whether this average is a good approximation to the isotropic velocity. Fortunately, there are global models of azimuthal anisotropy that can help address this concern [e.g., *Montagner and Tanimoto*, 1991; *Trampert and Woodhouse*, 1996]. Figure 14a shows examples of the 2ψ fast axis directions for a preliminary phase velocity model of *Trampert and Woodhouse* [1996]. Azimuthal anisotropy is large significant across much of Eurasia in this model. Note that the pattern of anisotropy changes appreciably between the 40 s and longer period maps. For example, in central Asia the pattern shifts from dominantly east-west to north-south. Also note that the amplitude of anisotropy is greater for the Love wave than the Rayleigh wave at each period. The model also contains a substantial 4ψ component. The uncertainty in the amplitude of the anisotropy is much larger than in the pattern of anisotropy, especially for the 4ψ component (J. Trampert, personal communication, 1997).

Similar to the synthetic experiments which test the effect of source mislocation and source group time shift on the estimated group velocity maps, we use *Trampert and Woodhouse's* [1996] model to estimate the bias in the isotropic maps caused by azimuthal anisotropy. Trampert and Woodhouse's model is for phase velocities, so its use for group velocities is not entirely straightforward. Since phase velocity kernels sample somewhat deeper than group velocity kernels at each period, we use the 40 s phase velocity maps of Trampert and Woodhouse as proxy for the 50 s group velocity maps and their 80 s Love wave phase velocity map for the 100 s Love wave group velocity map. However, we do use their 150 s Rayleigh wave phase velocity map for the 150 s Rayleigh wave group velocity map. Both 2ψ and 4ψ terms are included in the construction of the synthetic travel times which we then invert, exactly as the real data, at 50 s and 150 s for Rayleigh waves and at 50 s and 100 s for Love waves. The 4ψ component produces a small percentage of the bias except near the periphery of the maps.

Figure 14b presents estimates of the bias in the estimated isotropic maps caused by azimuthal anisotropy. Four features are worth noting. First, the amplitude of

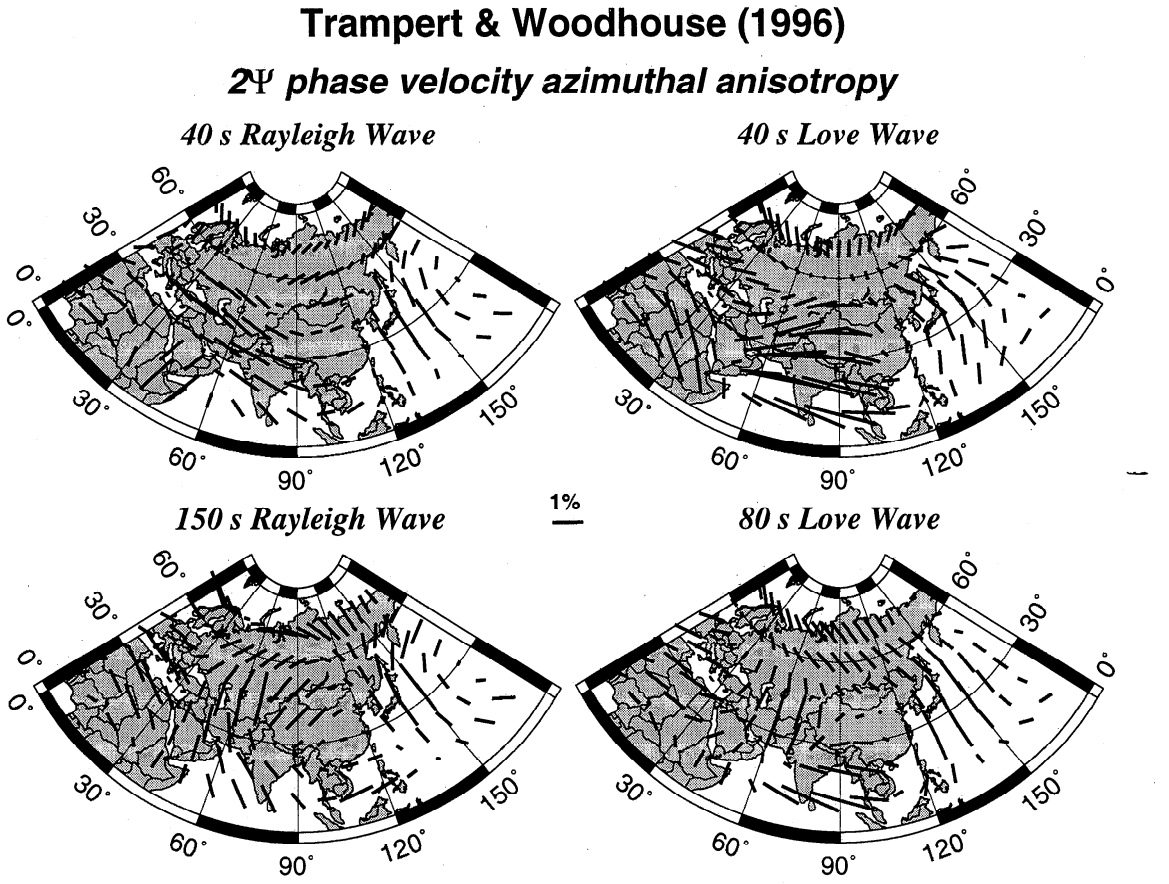

Figure 14a. The 2ψ fast axes from the model of phase velocity azimuthal anisotropy of *Trampert and Woodhouse* [1996]. A 1% velocity bar is presented for comparison in the center.

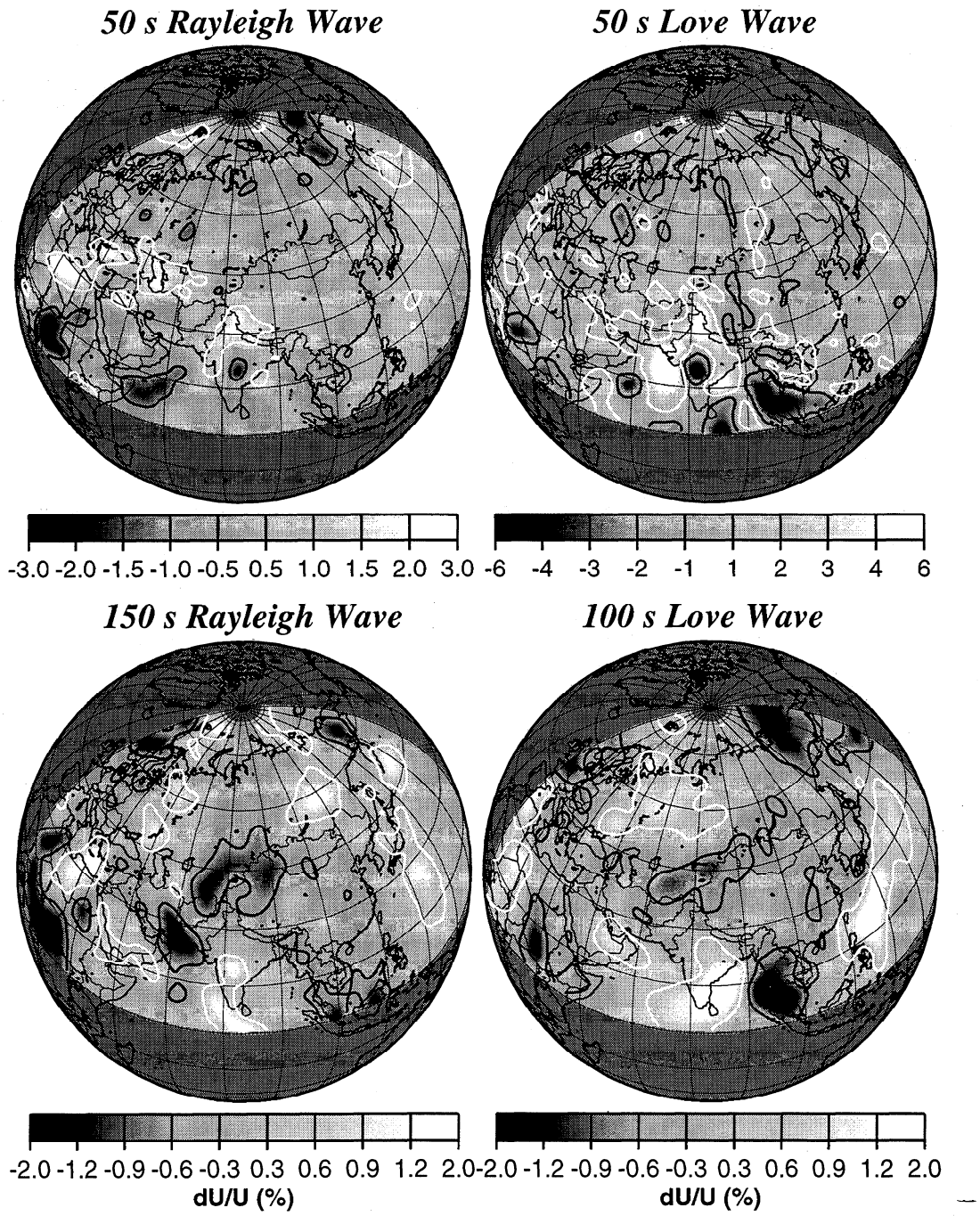

Figure 14b. Azimuthal anisotropy bias. Estimated bias from azimuthal anisotropy expressed as percent error relative to the average group velocity across the region of study for each period and wave type. The ±1% contours are drawn for the 50 s waves and the ±0.5% contours are indicated for the 100 s Love and 150 s Rayleigh waves.

the bias is typically larger for Love than for Rayleigh waves at each period. This is largely due to the fact that the amplitude of the azimuthal anisotropy for Love waves is larger in *Trampert and Woodhouse's* [1996] model, but is partially caused by the smaller number of Love wave than Rayleigh wave measurements. Second, the spatial size of the bias features are larger at the longer periods than at the shorter periods. This is caused by the fact that path lengths are typically greater at longer periods which tends to average out small-scale features. In addition, the longer-period maps are damped and smoothed somewhat more. Third, at 50 s period, the maximum bias occurs near the periphery of the maps, especially in the south, where azimuthal coverage is poorest, but at longer periods, bias is as likely to occur in the interior of the continent. This is because azimuthal distribution is typically worse in the interior at longer periods than at shorter periods.

Finally, the amplitudes of the bias features decrease with period. However, the amplitudes of bias relative to the signal levels in the estimated maps (Plates 2a-2c) are approximately constant. The average amplitude of maximum bias with respect to the maximum signal level is about 20%. A comprehensive study of the effect of azimuthal anisotropy on surface wave studies on a global scale has been performed recently by E.W.F. Larson et al. (Effects of a slight anisotropy on surface waves, submitted to *Geophysical Journal International*, 1997).

4.2.5. Summary. From these synthetic experiments we conclude that the largest source of bias from theoretical errors below about 100 s period probably results from azimuthal anisotropy. Owing to uncertainties in the amplitudes of *Trampert and Woodhouse's* [1996] model and the indirect relationship between phase and group velocity maps, the amplitude of the estimated bias is not well determined. However, the bias maps presented in Figure 14b are reasonable estimates. Since we presently only interpret features on the estimated group velocity maps with amplitudes larger than any of the bias estimates, it is unlikely that many of the interpretations in this paper are vitiated by theoretical errors. Nevertheless, to be able to interpret smaller amplitude features in future maps, it will be important to attempt to estimate azimuthal anisotropy simultaneously with transversely isotropic velocity. Bias from source mislocations and source group time shifts should be less significant than from azimuthal anisotropy, except in source regions near to the periphery of the maps at periods at and greater than about 100 s. The regions of greatest concern are near the Pacific rim. In the future, it would be prudent to include group time shifts in group velocity tomographic inversions.

5. Group Velocity Maps

Using the tomographic method described in section 3, we construct group velocity maps, which are smoothed using the results of the resolution analysis described in section 4, for Rayleigh waves at the following periods: 20, 25, 30, 35, 40, 50, 60, 70, 80, 90, 100, 125, 150, 175, and 200 s. The same periods are inverted for Love waves, except Love wave group velocity maps do not extend past 150 s period. A sampling of the estimated group velocity maps is presented in Plates 2a-2c. These maps represent lateral variations relative to the average across each map. (See Figure 15.) Group velocity curves at a few geographical locations, which have been constructed by combining all of the estimated group velocity maps, are shown in Figure 16. These maps are segregated roughly by tectonic or geologic type into three categories: sedimentary basins, continental plateaus or mountain ranges, and continental shields. The jerkiness in the curves results from small-scale inconsistencies between the group velocity maps at different periods. The observed curves are much smoother (e.g., Figures 3 and 5a).

At the time of writing, all group velocity maps are available and are regularly updated at the following web site: http://abdu.colorado.edu/geophysics/eurasia.dir/eurasia.html.

Our confidence in the longest-period maps shown in Plate 2 is not as high as in the shorter-period maps, in particular, at 200 s for Rayleigh waves and at 125 s for Love waves. There are two key reasons. First, accurate long-period measurements can only be obtained from large earthquakes ($M_s \gtrsim 6.0$), and the distribution of these events around Eurasia is not uniform and their numbers are not large. On average over the period of study (1988-1995), only about seven events per year with $M_s \geq 6.5$ occurred in the studied region. These events constitute less than 10% of our entire data set, which means that significant regions of Eurasia are not well covered at long periods, as the path coverage maps in Figure 7 demonstrate. Global-scale studies that utilize both major and minor arc wave packets demonstrate more uniform coverage across the continent [e.g., *Trampert and Woodhouse*, 1995, 1996; *Ekström et al.*, 1997] and should do better, in at least certain regions, at these very long periods. Second, as discussed in section 4.2, certain theoretical errors result in larger effects at long periods relative to the amplitude of the observed velocity perturbations. In summary, the advantages of continental-scale studies over global studies break down at periods beyond about 150 s for Rayleigh waves and about 100 s for Love waves.

Figure 17 shows the improvement in fit to the measured dispersion curves delivered by the estimated group velocity maps, expressed as the variance reduction relative to the average group velocity across each map (equation (4)) and the rms group velocity misfit (equation (5)). Variance reductions are more than 80% between 25 and 70 s period for both Rayleigh and Love waves. Variance reductions in excess of 80% continue for Love waves out to about 100 s period but decrease at longer periods since waves become increasing sensitive to the upper mantle which possesses smaller amplitudes of velocity variations than the crust. Since lateral variations in the group velocity maps have smaller am-

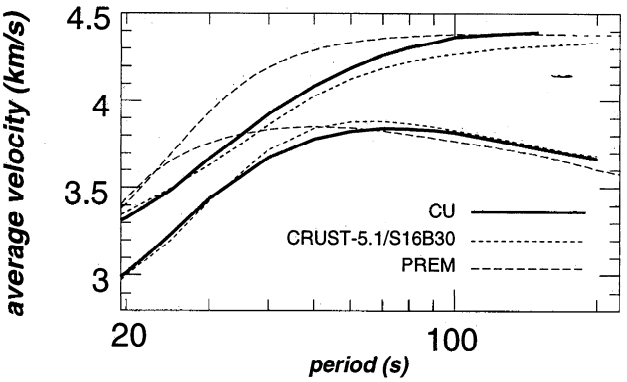

Figure 15. Average group velocity across the studied region (latitude 0°N - 85°N, longitude 0°E - 180°E) for our estimated group velocity maps (CU, solid lines), PREM (PREM, long dashed line), and the group maps predicted by a model composed of the crustal model CRUST5.1 and the mantle model S16B30 (CRUST5.1/S16B30, short dashed line).

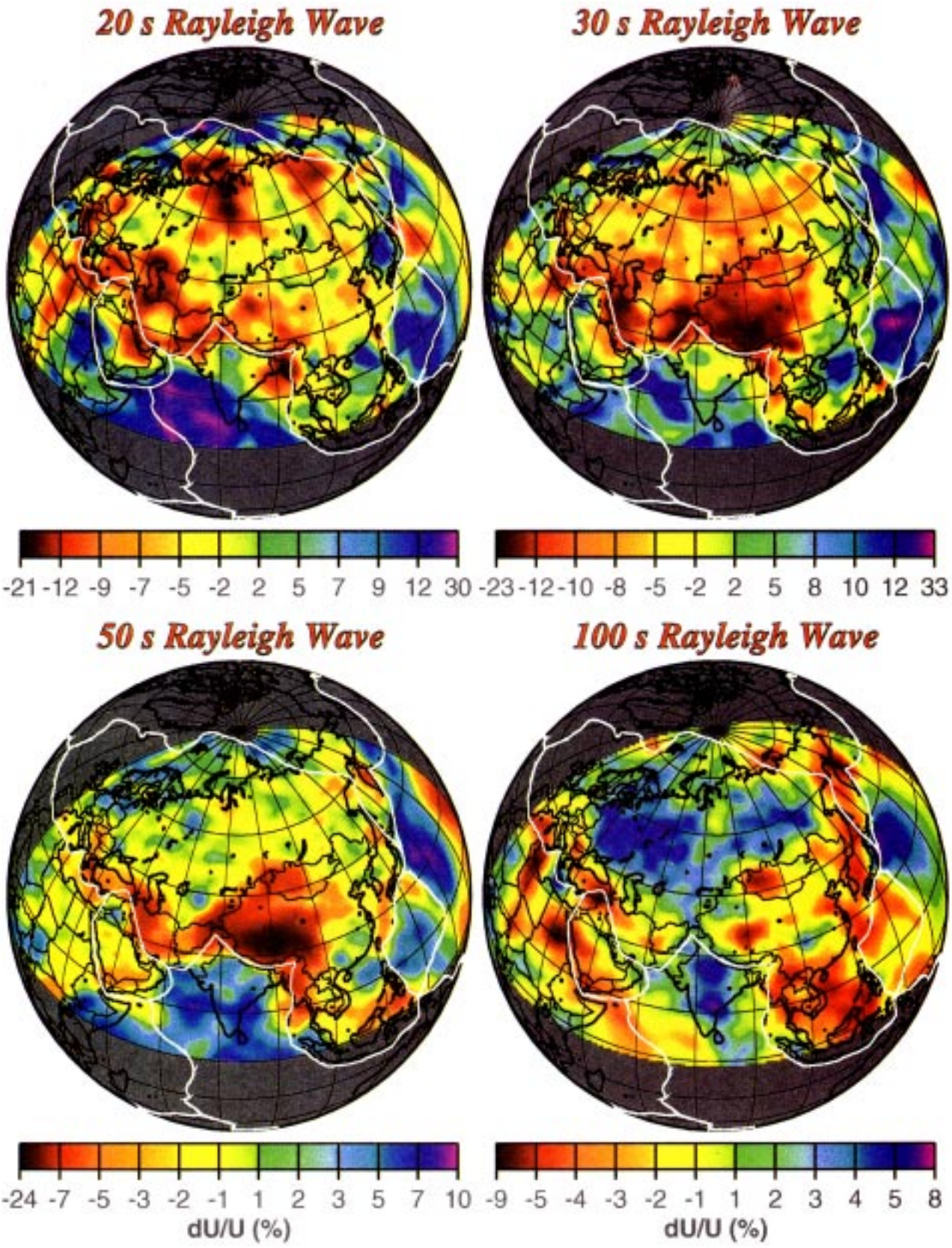

Plate 2a. Estimated group velocity maps across Eurasia for the 20 s, 30 s, 50 s, and 100 s Rayleigh waves.

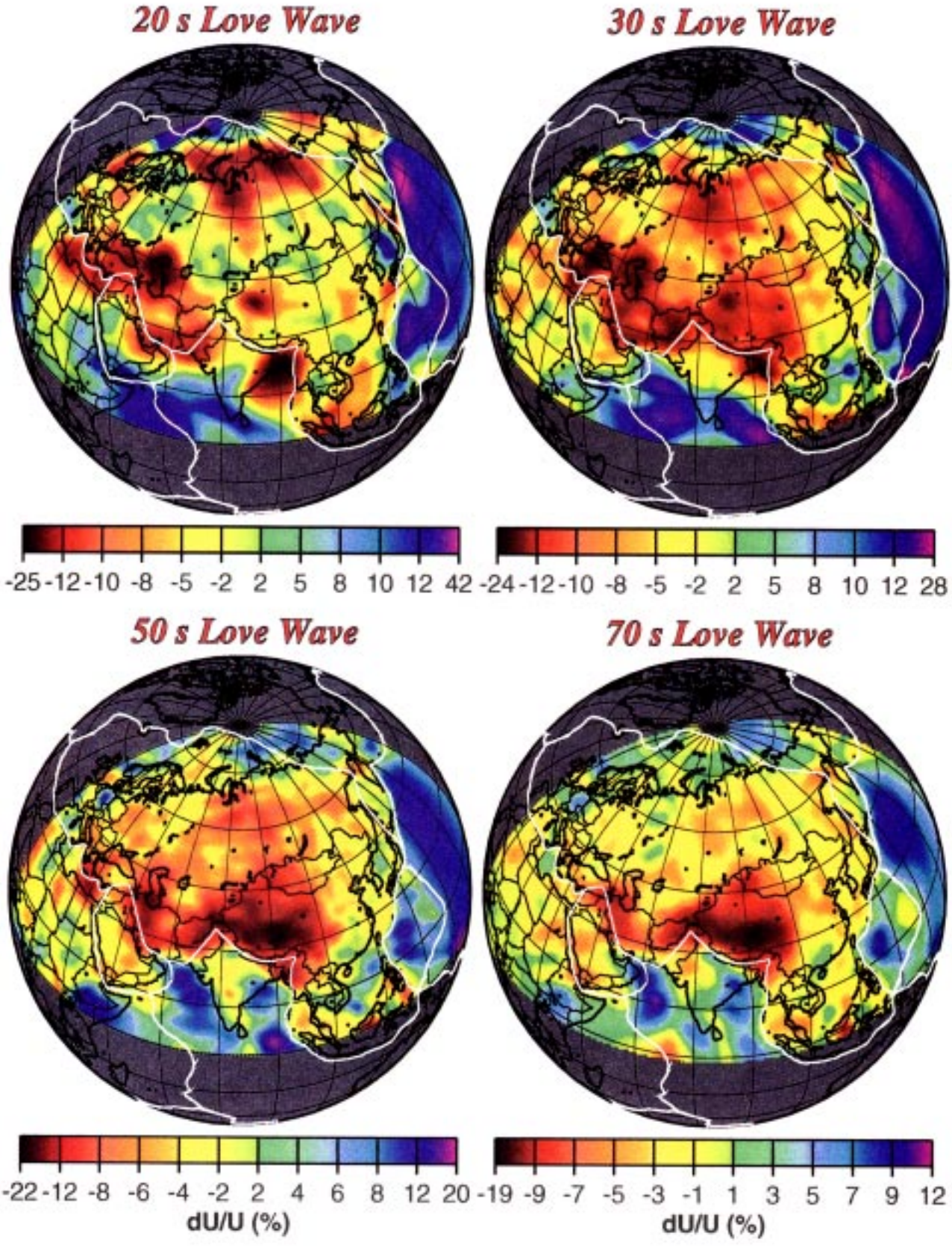

Plate 2b. Same as Plate 2a, except for the 20 s, 30 s, 50 s, and 70 s Love waves.

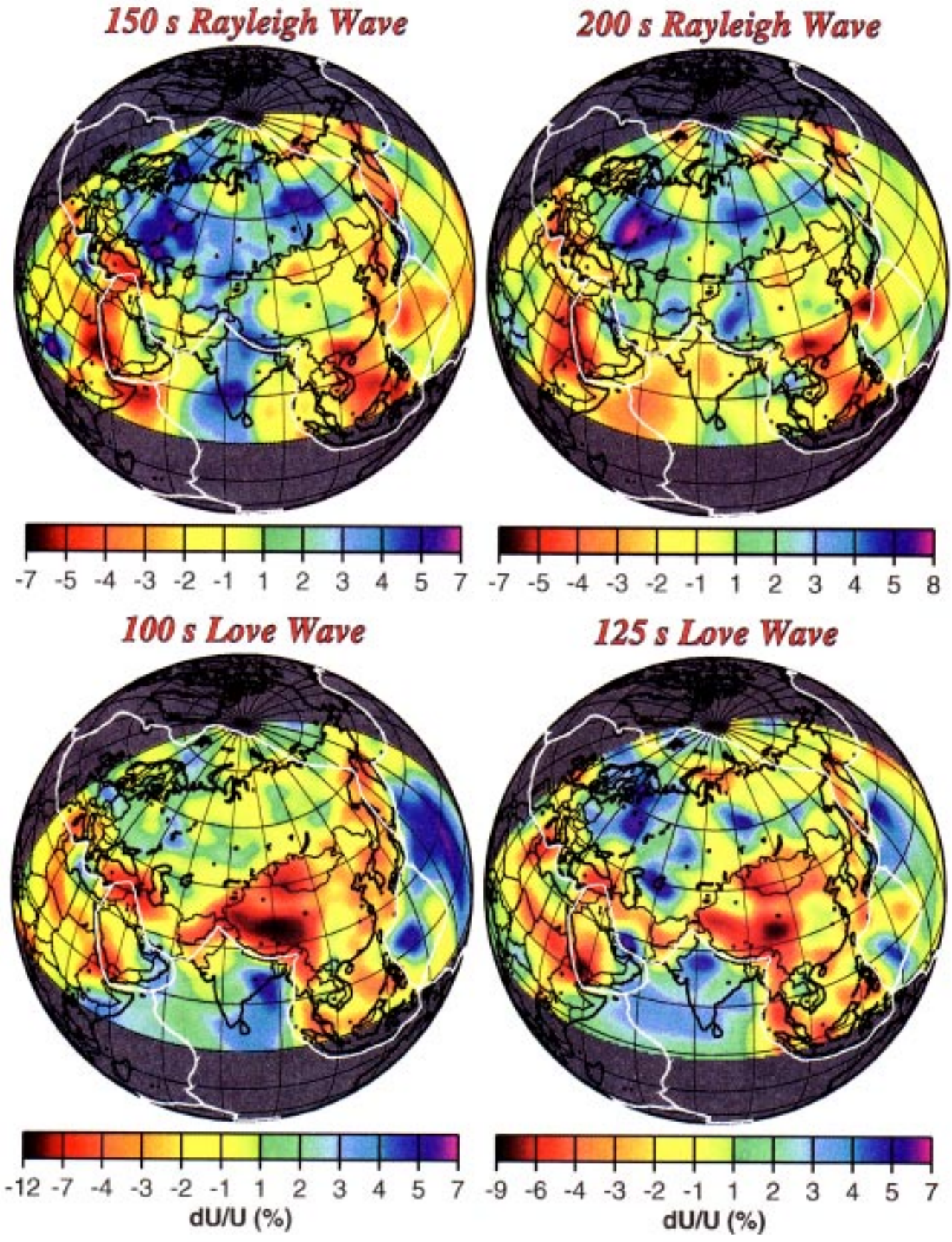

Plate 2c. Same as Plate 2a, except for the 150 s and 200 s Rayleigh waves and the 100 s and 125 s Love waves.

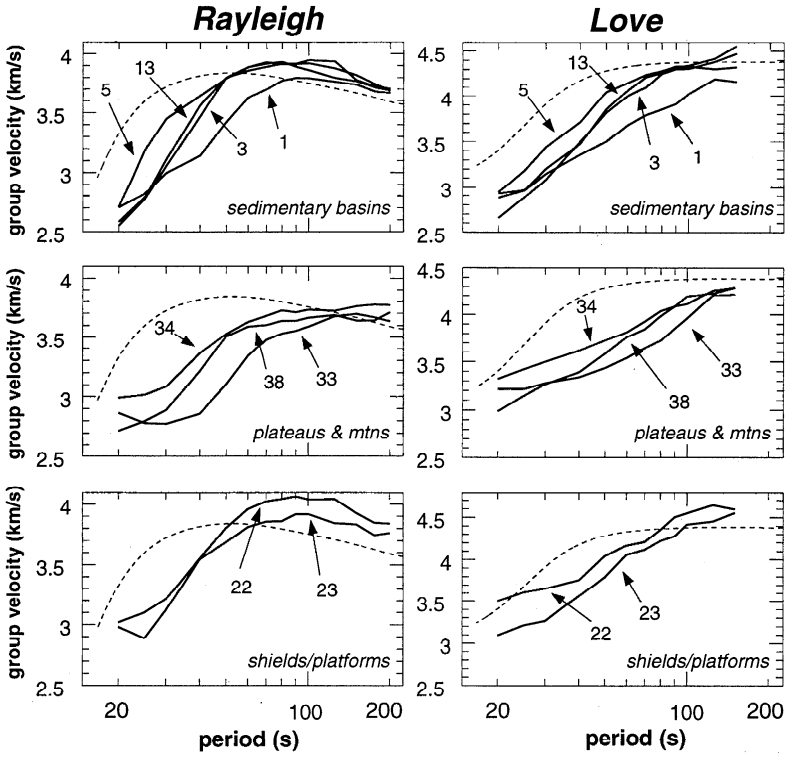

Figure 16. Group velocity curves ((left) Rayleigh and (right) Love) constructed by combining values at the specified locations from the estimated group velocity maps. The location key is in Figure 18. The curves are segregated by structural setting into three groups: sedimentary basins, mountain ranges or continental plateaus, and continental shields. The group velocity curve for PREM is shown as the dashed line on each graph.

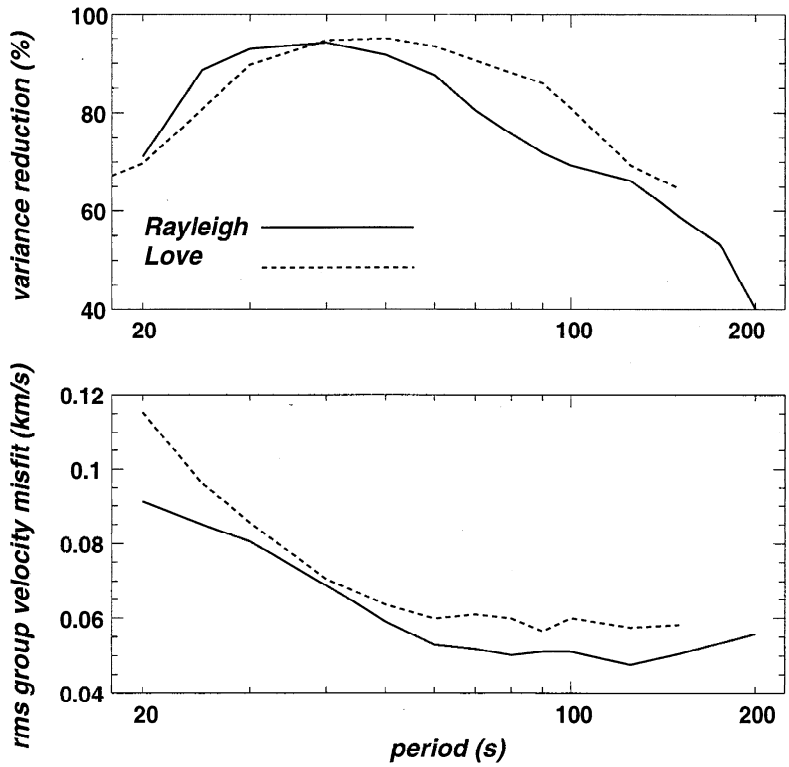

Figure 17. Two measures of misfit to our group velocity measurements for Rayleigh (solid lines) and Love (dashed lines) waves for our estimated group velocity maps. (top) Misfit is represented as variance reduction relative to the average across each map (equation (4)). (bottom) The rms group velocity misfit (equation (5)).

plitudes at longer periods, there is less signal to fit and therefore there is less reduction in variance. This degradation in variance reduction begins at shorter periods for Rayleigh waves since they sample deeper than Love waves at every period. Consistent with this is the fact that at the short-period end of the spectrum, absolute misfit is the greatest even though variance reduction continues to be high. Below about 30 s period, the decrease in variance reduction is probably due to off-great-circle propagation and scattering caused by sedimentary basins and other small-scale features. The onset of this degradation in variance reduction is at longer periods for Love waves since they sample more shallowly than Rayleigh waves at every period. For example, the 30 s Love wave is more strongly sensitive to sedimentary features than the 30 s Rayleigh wave. At 50 s and above, the absolute misfit is remarkably flat for both Rayleigh and Love waves, ranging between about 0.05 and 0.06 km/s.

Measurement uncertainties are also flat in this period range and average about 0.03 km/s, as Figure 5d shows. Thus misfits on average are about at the 1.5-2 σ level relative to the measurement uncertainties reported in Figure 5d. The uncertainties reported in Figure 5d are estimates of the repeatability of the measurements either across a regional array or for events in the same region. This uncertainty in velocity results principally from difficulties in measuring the time of the arriving wave packet accurately. These estimates do not include misfits caused by theoretical errors, such as those discussed in section 4.2. Signals of this magnitude can result from the remaining theoretical errors, mostly off-great-circle propagation at the short-period end of the spectrum and source group time shifts and azimuthal anisotropy at longer periods.

6. Discussion

Figure 15 compares the group velocities averaged across our estimated group velocity maps in the region of study (0°N - 85°N, 0°E - 180°E) with the group velocity from PREM [*Dziewonski and Anderson*, 1981] and the average group velocity in the studied region of the model CRUST5.1 in the crust [*Mooney et al.*, 1997] and S16B30 [*Masters et al.*, 1996] in the mantle. Not surprisingly, PREM poorly fits even average group velocities under largely continental regions, particularly below about 80 s period. The laterally inhomogeneous model (CRUST5.1/S16B30) predicts average group velocities much better with two key exceptions. First, for Rayleigh waves between periods of 40 and 80 s, group velocities predicted by CRUST5.1/S16B30 are on average too high. This is due to the fact that CRUST5.1 underestimates crustal thicknesses in structurally deformed areas and/or its lower crustal shear velocities are too high. Second, group velocities predicted by CRUST5.1/S16B30 are too low for Love waves, particularly at long periods. This principally results from the fact that CRUST5.1/S16B30 is an isotropic model and the observed dispersion curves show clear signs of polarization anisotropy (transverse isotropy). The model CRUST5.1/S16B30 provides a better fit to long-period Rayleigh waves than Love waves. It would be difficult for any isotropic model to fit both types of waves well.

Throughout the paper we have discussed a number of influences which tend to corrupt the resulting group velocity maps. These include, in addition to problems associated with path coverage, problems caused by theoretical assumptions, e.g., event mislocations, azimuthal anisotropy, off-great-circle propagation, and source group time shifts. These effects are all expected to be at levels below the major features in the group velocity maps that we interpret here and within the resolution estimates that we report. With this in mind, it is worthwhile pointing out some of the features that emerge in the group velocity maps, such as those in Plates 2a-2c, that appear to have clear structural causes. However, since the group velocity kernels in Figure 1 are complicated functions of radius, interpretation here should be considered preliminary in nature. In this interpretation, it is important to keep in mind path coverage and resolution (Figures 7 and 9) as well as the discussion of the effects of theoretical errors in section 4.2 (Figures 12, 13b, 14b).

Interpretation is based on plots of group velocity sensitivity kernels such as those shown in Figure 1. Figure 1 is computed for PREM, and continent-ocean variations in crustal thickness, in particular, change the details of surface wave sensitivities appreciably. Several rules of thumb generally hold, however. Group velocity sensitivity kernels are more complicated than phase velocity sensitivity kernels (e.g., they change sign) and are compressed nearer to the surface at each period. At a given period, Love waves sample more shallowly than Rayleigh waves and sensitivities for both types of waves compress toward the surface as period decreases. Consequently, everything else being equal, the best probe of sedimentary basins should be the shortest-period Love waves, which in this paper is at 20 s. However, the 20 s Rayleigh wave map is a better indicator of sedimentary basins since its resolution is significantly better than the 20 s Love wave. Rayleigh waves between 30 and 75 s are strongly sensitive to crustal thickness, and the 50 s Rayleigh wave map, to a fair approximation, can be seen as inversely related to Moho depth. That is, for a 50 s Rayleigh wave, low velocities result largely from thickened crust. Love wave sensitivity to crustal thickness maximizes nearer to 100 s period. At longer periods, the sensitivity of waves to crustal velocities and thicknesses diminishes. The uppermost mantle (80-150 km) is well represented in the 100 s Rayleigh wave map. The 150-200 s Rayleigh waves provide deeper sampling of the upper mantle sublithosphere.

Place names are presented in Figure 18, segregated by geological and tectonic type. Sedimentary basins and tectonic regions are taken from 3SMAC [*Nataf and Ricard*, 1996; *Kunin et al.*, 1987]. Plate 3 presents Rayleigh wave group velocity maps predicted by the model CRUST5.1/S16B30 at a variety of periods. The model CRUST5.1 is defined on a 5° grid, and the blocky nature of the predicted group velocity maps results from the grid defining the model.

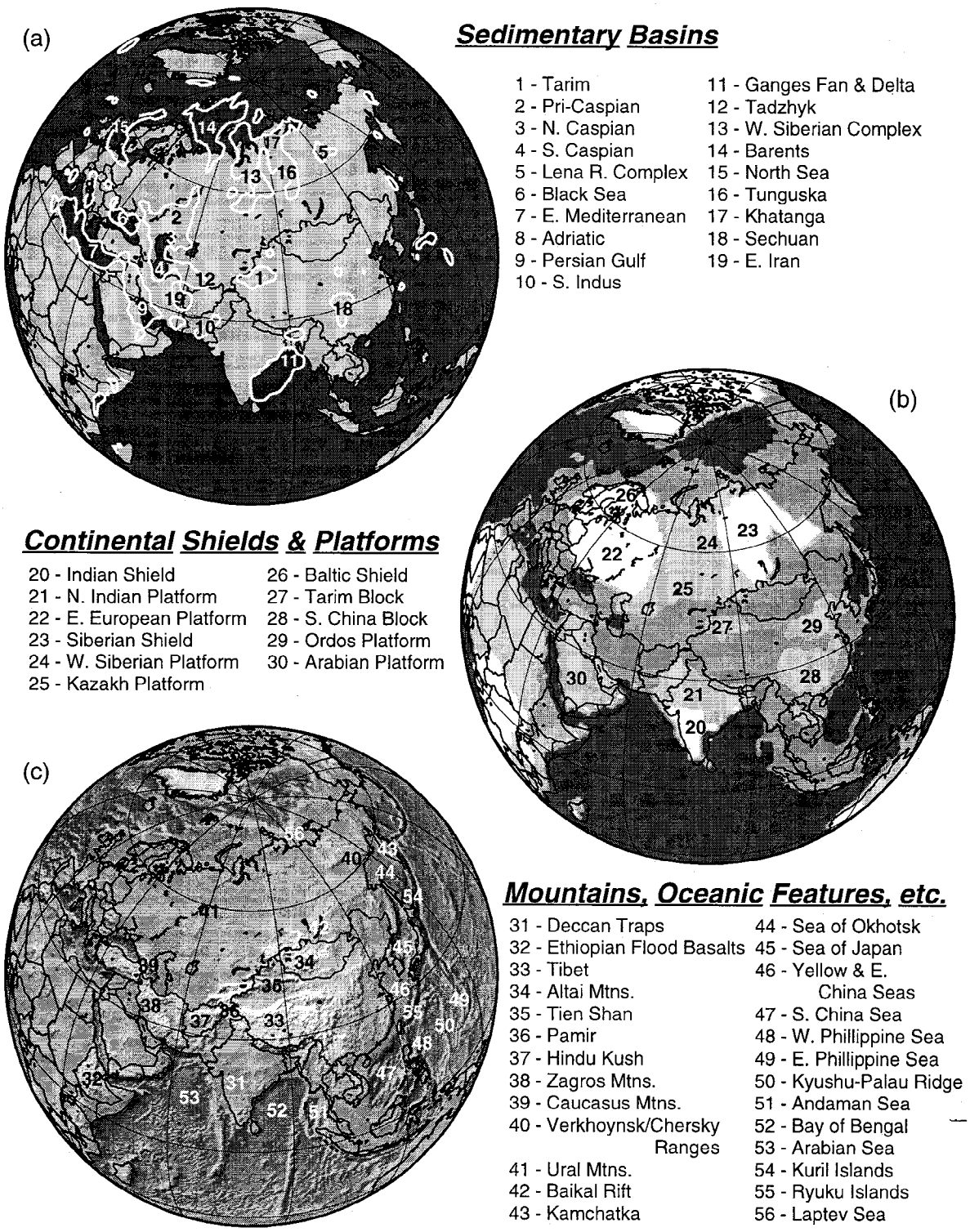

Figure 18. Place names. Sedimentary basin outlines (4 km isopach) and tectonic regions are taken from the 3SMAC model of *Nataf and Ricard* [1996]. Surface topography is from ETOPO-5.

6.1. Crustal Structures

Group velocity maps at periods below 100 s make excellent probes of crustal structures. Since Love wave group velocity sensitivities below about 30 s period and Rayleigh wave sensitivities below about 25 s are nearly entirely compressed within the continental crust, broadband measurements (<30 s to >100 s) of Rayleigh and Love wave group velocities can help to resolve crustal from mantle structures.

6.1.1. Sedimentary basins. Because of continuing rapid uplift across much of the Near East and

central Asia due to the collisions between the Eurasian Plate with the Arabian and Indian Plates, accumulations of relatively young sediments across Eurasia are considerably greater than on any other continent. The 20 s group velocity maps in Plates 2a and 2b display low-velocity anomalies associated with most of the known sedimentary basins across Eurasia. Low velocity anomalies are associated with the Tarim Basin, the Ganges Fan and Delta, the Persian Gulf, the Tadzhyk Depression, the southern Indus River, the north and south Caspian Sea, the Black Sea, the eastern Mediterranean Sea, the western Siberian sedimentary complex, the Pri-Verkhoyansky Foredeep along the Lena River and its tributary the Vilyuy River in eastern Siberia, the Barents Sea Shelf, the Sechuan Basin, the Adriatic Sea, and the North Sea.

Perhaps as interesting are the sedimentary basins that are not observed. These include the Tunguska and Khatanga Basins in Siberia and at least the northern part of the Pri-Caspian Depression. These basins all overlie shield areas and hence high upper crustal velocities, which obscure the low-velocity signature of the sediments. In addition, the Tunguska Basin has experienced massive basalt floods which interpenetrate the sediments.

Although the observed 20 s Rayleigh wave map (Plate 2a) and the map predicted from CRUST5.1/S16B30 in Plate 3 are well correlated, a number of significant differences are apparent. For example, the Tarim Basin lies largely between grid nodes of CRUST5.1, and is therefore nearly absent from this model. Also, the sedimentary velocity anomalies predicted by CRUST5.1 are generally much slower than observed. Perhaps this is because we have damped the estimated models, but it is not unlikely that the shear velocities in the deeper parts of the sedimentary basins in CRUST5.1 are too slow. Finally, CRUST5.1 predicts that the sedimentary basins in the Pri-Caspian and Tunguska regions should appear on the short period maps. The fact that they do not probably does not result principally from a problem with sedimentary structures in CRUST5.1, but rather with upper crustal velocities.

6.1.2. Ocean-continent variations. Inspection of the margins of the continent reveals information about the intrinsic resolution of the group velocity maps. For example, on the 30 s Rayleigh wave map in Plate 2a, the South China Sea, the Sea of Japan, and the Sea of Okhotsk are all imaged as relatively high velocities, whereas Kamchatka and the island arc comprising Japan, the Ryuku Islands, and Taiwan are clearly relatively low velocities. This observation is consistent with our earlier resolution analysis which resulted in claims of resolutions in this area of about 5°. The distribution of anomalies on the 30 s Rayleigh wave group velocity map in the Far East is partially the effect of crustal thickness variations, the thicker crust of the island arc manifests itself as reduced group velocities, but the higher crustal velocities of the marginal seas also contribute.

These observations are similar to the predictions from CRUST5.1/S16B30, displayed in Plate 3. There are several exceptions. (1) The map predicted by the model CRUST5.1/S16B30 under the marginal seas is much faster than observed, presumably due to shear velocities being too fast in the model or crustal thicknesses being somewhat too small in the model. (2) The observed map does not display the ability to resolve Korea from the Sea of Japan, the Yellow Sea, and the East China Sea that bound it. (3) However, our maps do show structural variations in the Philippine Plate that do not appear in CRUST5.1/S16B30. The Kyushu-Palau Ridge runs approximately north-south in the center of the Philippine Plate. The eastern Philippine Plate typically shows up as relatively low velocities in most of the group velocity maps at the short period end of our study. This may be due to sediment accumulated in the West Mariana Basin and Mariana Trough. However, since these low velocities persist to much longer periods (e.g., 70-125 s Love waves in Plates 2b and 2c) consistent with phase velocities reported by *Trampert and Woodhouse* [1996] and *Ekström et al.* [1997], it is likely that thicker crust exists on the east side of the Kyushu-Palau Ridge than on the west side.

6.1.3. Continental flood basalts. Massive basalt flows are known to exist in several regions across Eurasia, principally in northern Ethiopia, western India (Deccan Volcanic Province), and in central Siberia (Siberian Traps, Tunguska Basin). If unmodified by later sedimentation or thermal reworking, these regions should manifest themselves as high-velocity anomalies on the 20 s Rayleigh and Love wave maps (Plates 2a and 2b). The central Siberian flows in the Tunguska Basin [*Zonenshain et al.*, 1990] have been reworked since they were initially produced in the late Paleozoic, and they have also been obscured by large sedimentary basins that surround and interpenetrate them. Thus it is not surprising that this feature does not appear strongly on the estimated group velocity maps, although the basin is relatively fast on the 20 s Rayleigh wave map. On the other hand, the Ethiopian Flood Basalts [e.g., *Mohr*, 1983] and the Deccan Traps are associated with clear high-velocity anomalies on the 20 s Love wave map. Unfortunately, they are both in regions poorly sampled in this study at short periods. In the case of the Deccan Traps, the observed anomaly may be attributed to "leakage" of oceanic velocities onto the continent, but this explanation is less plausible for the Ethiopian/Sudaneses anomaly. Thus high-velocity anomalies on the short period maps in continental regions can reveal relatively young massive basalt flows.

The Ethiopian anomaly merges with another high-velocity anomaly to the north near the boundary between Egypt and the Sudan, perhaps most clearly seen on the 20 s Rayleigh wave map. This feature is not attributable to a basalt flow, but it is the site of a small Archaean shield which is probably the source of the observed anomaly. These higher velocities near the Egyptian-Sudanese boundary are predicted by the model CRUST5.1/S16B30.

6.1.4. Crustal thickness. The effects of variations in crustal thicknesses are best observed on the 50 s Rayleigh wave and 70 s Love wave maps in Plates

2a and 2b. Thick crust manifests itself as low-velocity anomalies on these maps. The strongest effects are in central Asia where the Moho extends to depths greater than 70 km. The most striking anomalies are associated with Tibet. The Pamir, near the northern boundary of Pakistan and Afghanistan, also display very low group velocities and, consequently, a significantly thick crust. Low velocities extend to the northeast from the Pamir into the Altai Range of Mongolia in a characteristic pattern first reported by *Wu and Levshin* [1994], and also extend southwest of the Pamir approximately following the boundary between Pakistan and Afghanistan associated with the Hindu Kush. The Tien Shan, Zagros, and Caucasus Mountains also display low-velocity anomalies. More subtle low-velocity anomalies are observed on the 50 s Rayleigh wave map associated with the Urals and the Verkhoyansk and Chersky Ranges in eastern Siberia.

In the Near East and central Asia there is qualitative agreement between the observed group velocity maps most sensitive to crustal thickness (e.g., 50 s Rayleigh in Plate 2a) and the prediction of CRUST5.1/S16B30 (Plate 3), but the outlines of Tibet are much more clearly delineated on the observed map than can be produced by a relatively coarse gridded model. Low velocity anomalies are also predicted by CRUST5.1/S16B30 associated with the Zagros and Caucasus Mountains.

6.2. Upper Mantle

As periods increase, the imprint of crustal structures on group velocity maps diminishes until, for Rayleigh wave maps at periods of 100 s and above, the signatures of upper mantle structures dominate the group velocity maps. We concentrate discussion here on the 100 s and 150 s Rayleigh wave maps shown in Plate 2c which we believe most robustly reveal information about the upper mantle.

6.2.1. Archaean shields/continental roots. Continental roots can be seen in various regions around Eurasia on the 100 s and 150 s Rayleigh wave maps. The largest features are the two Archaean shields underlying the Eastern European Platform and the Siberian Shield, separated by the Urals. These roots also are apparent on the long-period group velocity maps predicted by CRUST5.1/S16B30, since they compose part of the mantle model S16B30. The Tornquist-Teisseyre Zone (TTZ) [e.g., *Hurtig et al.*, 1979; *Guterch et al.*, 1986; *Pedersen et al.*, 1994; *Zielhuis and Nolet*, 1994; *Lomax and Snieder*, 1995; *Alsina and Snieder*, 1996], a tectonic lineament striking northwest-southeast from southern Scandanavia through Poland to the Black Sea, is also seen on our maps. The TTZ marks the transition from the thicker and older (hence faster) Eastern European Platform to the thinner and younger (hence slower) lithosphere of western Europe. The TTZ appears as a sharp gradient on the 100-200 s Rayleigh wave maps. Several smaller shields or lithospheric blocks are also seen as high-velocity anomalies on the 100 s and 150 s Rayleigh wave maps, such as the Baltic Shield, the Tarim block, the Kazakh Platform, the Indian Platform and Shield, and the South China Block. These features are too small to appear in global models such as S16B30.

6.2.2. Pacific rim backarc. After the high-velocity anomalies due to the continental roots underlying the Eastern European Platform and the Siberian Shield, the most striking feature on the long-period maps may be the low-velocity arc rimming the continent on its eastern edge. This feature extends, essentially uninterrupted, from Kamchatka to Indochina, although the largest velocity anomalies appear to underlie Kamchatka, the backarc west of Japan, and Indochina.

The Pacific Rim low-velocity anomaly, in a more poorly resolved form, appears in nearly all of the recent global mantle models and may be attributable to the response of the mantle to backarc spreading or increased volatile content due to partial melting of the subducted slabs. There is qualitative agreement, for example, between the observed 100 s Rayleigh map in Plate 2c and the map predicted from CRUST5.1/S16B30 in Plate 3. The biggest differences appear to be resolution and amplitude, which may be due to the greater damping necessary in the construction of global mantle models. The amplitudes of the velocity anomalies in S16B30 are lower, and relatively small features, such as the East China Block, are missing in the global models. As discussed above, the fact that crustal shear velocities in the marginal seas appear to be too high in CRUST5.1 results in the crustal part of the model continuing to imprint the 100 s Rayleigh wave map in Plate 3 under the marginal seas. The observed 100 s Rayleigh wave does not display the continued signature of crustal features in this region.

6.2.3. Plate boundaries. Several significant features are apparent at plate boundaries on the long-period Rayleigh wave maps. High-velocity anomalies are associated with known subduction occurring in the eastern Mediterranean, near the India-China border south of Tibet, and along the Pacific Plate boundary east of Japan. It is tempting to conclude that these anomalies are the signature of subduction in these regions or at least of a thickened lithosphere. These features are spatially too small to be included in the model S16B30.

There are several low-velocity anomalies observed in the 100 s and 150 s Rayleigh wave maps that are worth mentioning. None of these anomalies underlies convergent plate boundaries, and the mantle structures that produce them are not likely to be the same as at convergent boundaries. The first is in eastern Turkey under the Anatolian Fault Zone, which marks the collision zone between the Arabian and Eurasian Plates. The second is in the Laptev Sea associated with the southeastern edge of the Arctic spreading center. The third is under the Red Sea. Path coverage and expected resolution in the first of these regions are good but are less so in the other two regions. Although the first two of these features are not apparent in the mantle model S16B30, the third is. In fact, low-velocity anomalies underlying the Afar Triangle and extending north along the western edge of the Red Sea appear in the uppermost mantle in most of the recent global mantle models. These

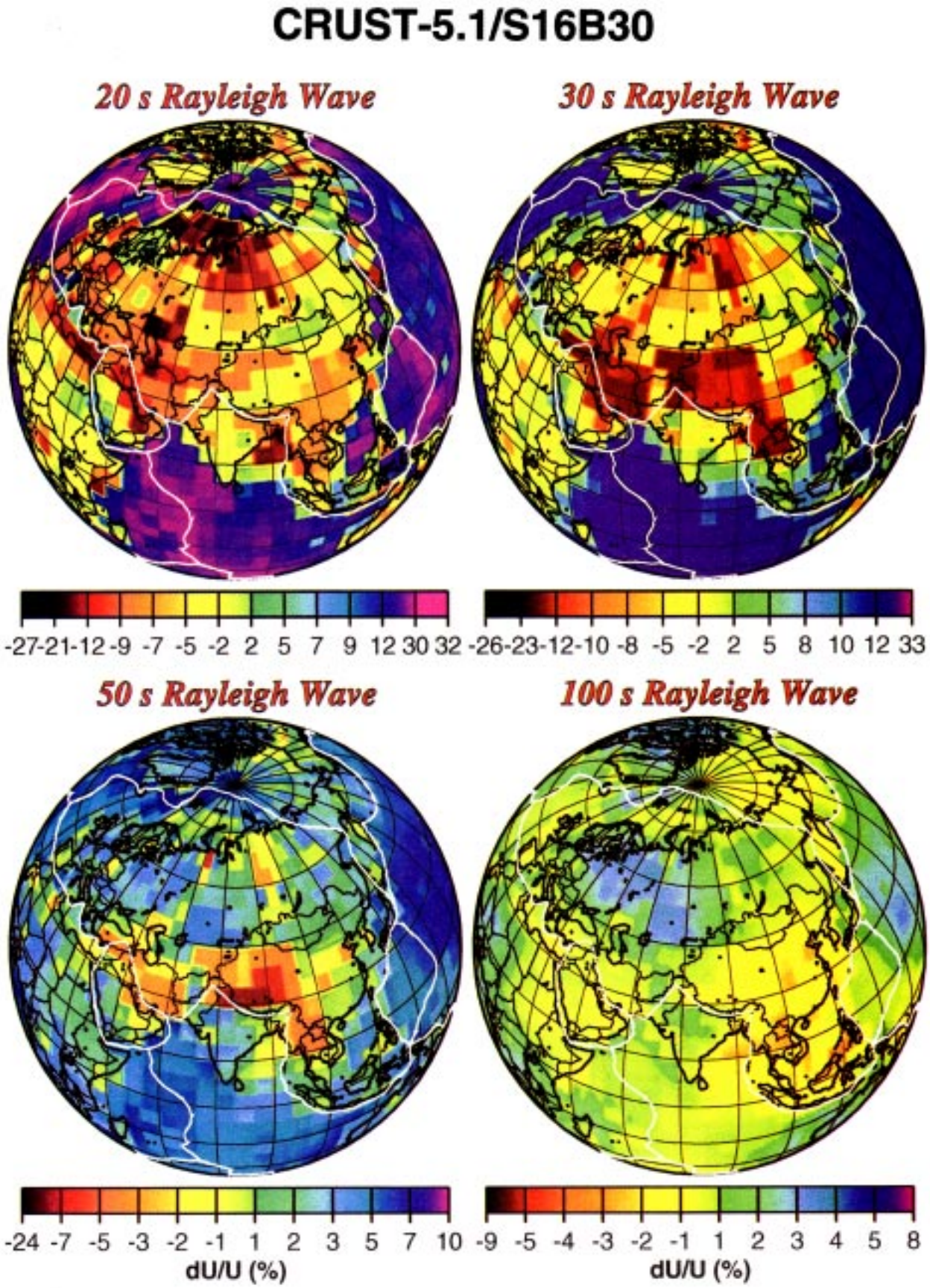

Plate 3. Rayleigh wave group velocity maps predicted by the model CRUST5.1/S16B30 at the indicated periods. The velocity scales are the same as on the observed maps in Plates 2a-2c, except for the maximum and minimum values.

anomalies have been interpreted as the head of the Afar Plume. The resolution and data coverage at long periods near the southern rim of our maps in East Africa are poor, and we do not assign significance to any geographical variations in the location of the "Red Sea" low-velocity anomaly among our group velocity maps or with those predicted by mantle models.

Also worthy of note is the low-velocity anomaly on the 100 s Rayleigh wave map in northern Tibet. Northern Tibet is marked by volcanism and elevated heat flow and has been hypothesized to be the site of thinned lithosphere [e.g., *Zhao and Xie*, 1993; *McNamara et al.*, 1995] created, perhaps, by lithospheric delamination or gravitational instability [*Molnar et al.*, 1993]. The 100 s Rayleigh wave map is consistent with these observations and interpretation. The low-velocity anomaly in western Mongolia may or may not be an associated feature.

6.3 Misfit Compared with the Model CRUST5.1/S16B30

As previously discussed in sections 6.1 and 6.2, there is qualitative agreement between the observed group velocity maps and those predicted by CRUST5.1/S16B30. Disagreements are mostly in amplitude and in certain features, particularly in the upper mantle, which are too small to appear in S16B30. We have concluded that: sedimentary shear velocities in CRUST5.1 tend to be too low in deep basins, the crustal shear velocities in the marginal seas are too high in CRUST5.1, crustal thicknesses in CRUST5.1 across much of the continent are somewhat too small and/or the lower crustal velocities are too high, upper mantle structures in S16B30 are too small in amplitude on average, and certain observed upper mantle features are spatially too small to be contained in S16B30. The question we ask here is, what is the effect of these observed differences on the fit to the group velocity observations? As discussed earlier, small-scale anomalies only minimally affect the measures of misfit considered here, so these misfit comparisons dominantly reveal information about the large-scale features on the observed maps.

This question is addressed by Figure 19 which presents the variance reduction and rms group velocity misfit between the observed group velocity curves and those predicted by our maps and the group velocity maps predicted by CRUST5.1/S16B30. The variance reductions reported in Figure 19 differ from those in Figure 17 in that here we take as the reference model, U_0, the group velocity curve predicted by PREM, whereas in Figure 17 we took the reference model to be the average velocity observed across the continent at each period. Thus

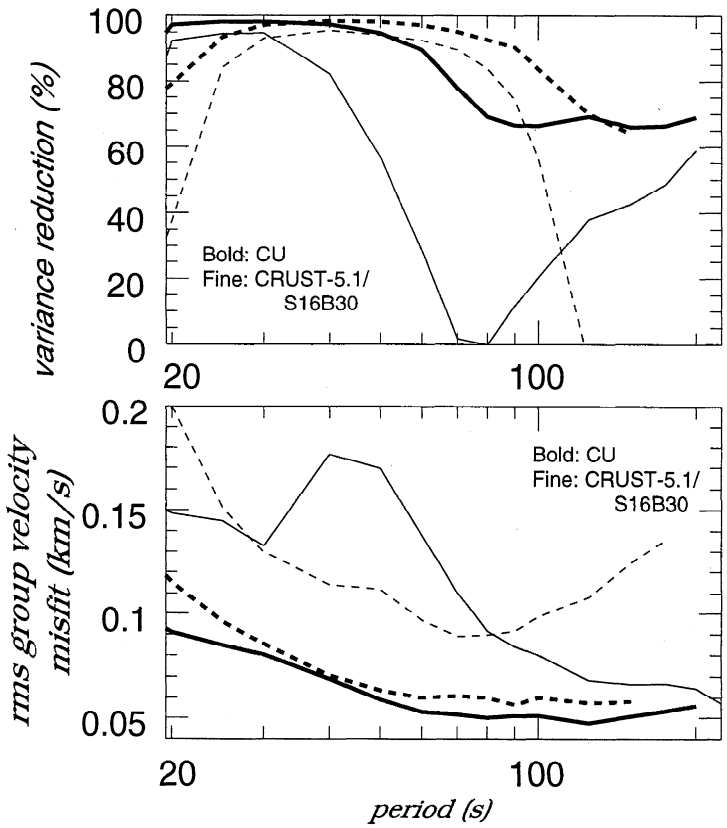

Figure 19. Two measures of misfit to our group velocity measurements for Rayleigh (solid lines) and Love (dashed lines) waves for two different sets of group velocity maps. Thick lines are for our group velocity maps and thin lines are for the group velocity maps predicted by CRUST5.1/S16B30. (top) Misfit is represented as variance reduction relative to the group velocity from PREM. These variance reductions differ from those in Figure 17 since the reference values used in the figures differ. (bottom) Misfit is the RMS group velocity misfit (equation (5)).

we get larger variance reductions here than in Figure 17. The rms group velocity misfits for the observed group velocity maps are the same in Figures 17 and 19, however.

Variance reductions to the observed group velocity measurements provided by CRUST5.1/S16B30 are large and positive for both Rayleigh and Love waves across most of the band. Indeed, variance reductions are in excess of 80% for Rayleigh waves between 20 and 40 s period and for Love waves between 25 and 80 s. Both observed and predicted variance reductions decrease at longer periods because of a decrease in signal level. The principal exceptions are for Love waves at periods greater than about 80 s and for Rayleigh waves from 50 to 100 s. The degradation in misfit of CRUST5.1/S16B30 to the long period Love waves is largely due to polarization anisotropy since this is an isotropic model which cannot fit Rayleigh and Love waves well simultaneously. Rayleigh wave variance reductions for CRUST5.1/S16B30 begin to decrease beyond about 30 s period and minimize between 70 and 80 s period. This is caused by the strong sensitivity of Rayleigh waves to crustal thickness in this period range and the fact that CRUST5.1/S16B30 appears to underpredict crustal thicknesses and/or overestimates lower curstal shear velocities across much of Eurasia. The increase in absolute misfit for CRUST5.1/S16B30 between 40 and 70 s period is due to the average group velocity across the continent in the model being in error, as shown in Plate 3. Thus we attribute this increase in absolute misfit to errors in the average value of group velocity across the model. This is not reflected exactly in variance reduction since signal level increases in this period range which somewhat offsets the increased misfit.

The observed maps do, however, fit the group velocity measurements significantly better than the predictions from CRUST5.1/S16B30. Recall that in section 2 we estimated the observational error at about 0.03 km/s, so the estimated group velocity maps misfit the data at about the 1.5-2σ level and CRUST5.1/S16B30 misfits at least at the 4σ level below about 80 s period for Rayleigh waves and greater than 3σ across the entire band for Love waves, especially at long periods. This should not be surprising for three reasons. First, CRUST5.1 is principally a v_p model in which the v_s variations have been approximated by use of a constant Poisson's ratio, and much of the crust in Eurasia is relatively unconstrained by seismological data at the disposal of the authors of CRUST5.1. Second, CRUST5.1 is defined on a 5° grid in which velocities are assumed constant within each cell. Finally, the mantle part of the model, S16B30, displays much longer wavelengths and lower amplitudes than what is implied by the observed long-period group velocity maps.

7. Conclusions

We have reported the results of a systematic study of broadband Rayleigh and Love wave dispersion across Eurasia. We believe, and argue here, that this study represents a significant improvement in the understanding of surface wave dispersion across this continent. However, the results presented here are not complete. The methods described may continue to be applied across Eurasia to new and accumulating data in order to improve resolution and reliability further. The methods are already being applied successfully to other continents (e.g., Antarctica [*Ritzwoller et al.*, 1996c]; South America [*Vdovin et al.*, 1996]) and can be developed further in the ways described below.

There are three main reasons why we believe that this study represents a significant improvement in the understanding of Eurasian surface wave dispersion. The first has to do with the data used. This study is broader band, displays denser and more uniform data coverage, and demonstrates higher resolution than previous studies that have been performed on this scale. Resolutions at most periods for the majority of the continent lie between 5° and 7.5°. Second, the group velocity maps reveal the signatures of known geological and tectonic features never before revealed in surface wave studies on this scale. This both lends credence to the maps and spurs interest in their use to infer information about the features that are observed. Observations at short and intermediate periods (~20-80 s) are providing entirely new constraints on crustal structures, and the long-period observations ($\geq$100 s) are yielding higher-resolution information about the deep lithosphere and upper mantle. Finally, the group velocity maps provide a significant improvement in fit to the observed dispersion curves. This is particularly impressive when compared to misfits from existing mantle and crustal models.

Concerning the crust, observed group velocity anomalies include information about sedimentary velocities and thicknesses, crustal velocities, and Moho depths. The dispersion signatures of numerous sedimentary basins across the continent and off the coast are displayed clearly on the-short period (20-30 s) group velocity maps (e.g., Tarim Basin, Ganges Fan and Delta, Persian Gulf, Tadzhyk Depression, southern Indus River, northern and southern Caspian Sea, Black Sea, eastern Mediterranean Sea, western Siberian sedimentary complex, Lena River Complex, Barents Sea Shelf, Sechuan Basin, Adriatic Sea, North Sea). Although the effects of sedimentary basins on intermediate period surface wave velocities and polarizations have been reported before (e.g., Barents Sea Shelf [*Levshin and Berteussen*, 1979]; Caspian Sea [*Levshin et al.*, 1994]), we are not aware of a similarly comprehensive study on a continental scale. In addition, high-velocity anomalies on the short period maps are observed for three continental regions of massive basalt flows (Siberian Traps, Ethiopian Flood Basalts, Deccan Traps). The significance of the observation of the surface wave signature of known massive basalt flows associated with the break up of Gondwanaland is probably not greatest for its application to Eurasia but lies in its potential application to other more poorly understood continents, in particular Antarctica [e.g., *Ritzwoller et al.*, 1996c]. Perhaps the most striking feature on any of the group

velocity maps is the low-velocity anomalies that appear on both the Rayleigh (30-90 s) and Love (40-125 s) wave maps associated with the thickened crust of central Asia, in particular Tibet. Such low-velocity anomalies for Tibet have been presented before [e.g., *Feng and Teng*, 1983a; *Wu and Levshin*, 1994], but the present study provides a broader frequency band, better resolution, and larger spatial coverage than previous studies. Similar dispersion anomalies for other regions of thickened crust are also revealed (e.g., Altai Range, the Hindu Kush and Pamir, Zagros and Caucasus Mountains, more subtle anomalies associated with the Urals, Verkhoyansk/Chersky Ranges) as well as variations in crustal thicknesses between continental and oceanic crust (e.g., the arc composed of Kamchatka, Kurile Islands, Japan, the Ryuku Islands, and Taiwan). The breadth of the frequency band over which the dispersion maps are produced holds the promise for resolving these crustal structures from one another and from upper mantle structures during structural inversion for a shear velocity model.

Concerning the lower lithosphere and upper mantle, observed group velocity anomalies include information about backarc spreading, continental roots, the depth extent of the lithosphere, downgoing slabs, and perhaps the upper reaches of a mantle plume. The observed long period Rayleigh wave maps (e.g., 100 s) provide a much sharper view of the linear low-velocity anomaly that rims the continent in the Far East, which may be caused by the mantle's response to backarc spreading, than global models [e.g., *Su et al.*, 1994; *Masters et al.*, 1996]. Continental roots under shields have emerged in recent global models [e.g., *Trampert and Woodhouse*, 1995; *Masters et al.*, 1996; *Ekström et al.*, 1997]. The large Eurasian shields (Eastern European Platform, Siberian Shield, Indian Shield) are very clearly imaged on the long-period maps presented here, as are other deep lithospheric blocks, such as the Baltic Shield, the Kazakh Platform, and the Tarim and the South China Blocks, which are too small to be seen in the global models. The Tornquist-Teisseyre Zone is clearly imaged as a high gradient region. High-velocity anomalies are also associated on the long period maps with descending slabs at the Pacific Plate margin, at the plate boundary between India, China, and Pakistan, and under the eastern Mediterranean Sea. The "Red Sea" low-velocity anomaly, which appears clearly but more diffusely in many global models and has been hypothesized to result from the Afar Plume [*Makris and Ginzburg*, 1987; *Hill et al.*, 1992], is well seen on the long-period maps presented here, centered on and just west of the Red Sea.

The group velocity maps we present here provide a substantial improvement in fit to the observed data relative to any laterally homogeneous model. Variance reductions relative to PREM are about 90% at the short-period end and reduce to about 70% at the long-period end of the study. To put this in context, comparisons are made with the variance reductions from a new high quality laterally inhomogeneous model, CRUST5.1/S16B30 [*Mooney et al.*, 1997; *Masters et al.*, 1996]. CRUST5.1/S16B30 does a good job of fitting the observed group velocity curves and detailed comparisons between the observed group velocity maps and those predicted by CRUST5.1/S16B30 demonstrate a good qualitative agreement. Not surprisingly, however, the observed maps do significantly better in fitting the data, and several characteristics of CRUST5.1, in particular, appear to require future improvement. We believe that in CRUST5.1 shear velocities are too low in the deep parts of sedimentary basins (perhaps caused by inaccurately modeling the increase in shear velocities due to sedimentary compaction), the crustal shear velocities in certain marginal seas are too high, and crustal thicknesses across much of the continent are too small and/or lower crustal shear velocities are too high. Irrespective of these comments, CRUST5.1/S16B30 represents a tremendous improvement over previous global models of the crust and uppermost mantle under Eurasia and is an excellent basis for future research. We have derived added confidence in the veracity of the observed group velocity maps from the fact that the observed and predicted maps agree well qualitatively, but the observed maps provide a large improvement in fit to the data.

Although we have argued at some length that this study represents a significant step toward an understanding of Eurasian surface wave dispersion, there remain several shortcomings. In particular, resolution and bias have not yet been optimized, for example, by modeling off-great-circle propagation, utilizing amplitude, polarization [e.g., *Laske and Masters*, 1996], and/or phase information, or making use of all of the available broadband data. These shortcomings point the way for future research. First, phase velocity measurements have already been made along with the group velocities, and phase velocity maps will be constructed soon. Second, more waveform data will be analyzed and added to the tomographic inversion. Our studies in central Asia have shown how important it is to utilize regional network and array data to improve resolution, particularly at short periods [*Ritzwoller et al.*, 1996b]. The use of data from the new network in Saudi Arabia [*Vernon et al.*, 1996], new broadband stations installed by the Japanese in the Far East (e.g., POSEIDON), the NARS network in European Russia, the Ukraine, and Belorussia [*Snieder and Paulssen*, 1993], national regional networks such as the German Regional Seismic Network [e.g., *Krueger and Stammler*, 1996], past PASSCAL experiments (e.g., Tibetan Plateau, Pakistan, Lake Baikal), and broadband components of U.S. Department of Defense arrays would help to improve resolutions in Europe, central Asia, the Middle East, and the Far East. Resolution in northern Asia can be improved if nearly meridional paths are analyzed. These paths can come from the analysis of data from recently installed north eastern Siberian GSN stations (e.g., TIXI, BILL), from the Canadian National Seismic Network, and from the U.S. National Seismic Network for events which take place across Eurasia. Third, the

effects of theoretical errors can be reduced further by incorporating group source time shifts above 40 s period in future tomographic inversions and by attempting to estimate azimuthal anisotropy simultaneously. Finally, the estimated dispersion maps (group and phase) may be inverted for shear velocity models across Eurasia. These studies have begun for central Asia [e.g., *Ritzwoller et al.*, 1996a].

Acknowledgments. Many people and organizations contributed to this study. We are grateful to C. Archambeau for suggesting this collaboration in 1991. A. Curtis, J.-J. Lévêque, II. Paulssen, and R. Snieder provided very helpful reviews. O. Vdovin performed much of the azimuthal anisotropy bias experiment and helped in making some figures. J. Trampert and J.-P. Montagner provided azimuthal anisotropy models. J. Woodhouse and R. Hermann provided eigenfunction codes. G. Laske, W. Mooney, S. Johnson, and G. Masters provided the crustal model CRUST5.1 and the mantle model S16B30 that we used as a touchstone throughout this study. Our analysts L. Ratnikova, S. Smith, D. Tremblay, C. Lee, M. Silitch, R. Kelly, and M. James made all of the measurements that form the backbone of this research. D. Quinlan and D. Harvey provided a great deal of software and data management advise and support. Much of the database software was written with Datascope [*Quinlan*, 1994]. A.A. Egorkin and M.P. Barmin played central roles in the development of software used in several aspects this study, in particular in developing the UNIX version of FTAN and in code used in the resolution analysis. We would like to thank T.B. Yanovskaya and P.G. Ditmar for generously supplying their group velocity tomography code. R. Engdahl gave us tables of ISC event locations as well as his relocations which together have helped us gauge the effect of epicenter differences between catalogues on the estimated group velocity maps. We enjoyed many valuable conversations with J. Rial. Most of the data were acquired from the IRIS-DMC and the Geoscope Data Center (G. Roult). We are grateful to a number of individuals at regional and global data collection centers who really control the quality of the data used in this study. These include the groups at UCSD (IRIS/IDA, J. Berger, P. Davis; KNET, F. Vernon), Albuquerque Seismic Laboratory (IRIS/GSN, R. Woodward), LDEO (KAZNET, W.Y. Kim), and MEDNET (A. Morelli). All maps were generated with the Generic Mapping Tools (GMT) data processing and display software package [*Wessel and Smith*, 1991, 1995]. This research was supported by AFOSR contract F49620-95-1-0139, AFTAC contract F19628-95-C-0099, a small grant from IRIS, and NATO linkage grant N950775 between the University of Colorado, Boulder and the Institute of Earthquake Prediction Theory and Mathematical Geophysics, Russian Academy of Sciences, Moscow.

References

Alsina, D., and R. Snieder, Constraints on the velocity structure beneath the Tornquist-Teisseyre Zone from beamforming analysis, *Geophys. J. Int.*, *126*, 205-218, 1996.

Backus, G., and J.F. Gilbert, Resolving power of gross earth data, *Geophys. J. R. Astron. Soc.*, *16*, 169-205, 1968.

Backus, G., and J.F. Gilbert, Uniqueness in the inversion of inaccurate gross earth data, *Philos. Trans. R. Soc. London, Ser. A*, *266*, 123-192, 1970.

Bird, P., and M.N. Toksoz, Strong attenuation of Rayleigh waves in Tibet, *Nature*, *266*, 161-163, 1977.

Bourjot, L., and B. Romanowicz, Crust and upper mantle tomography in Tibet using surface waves, *Geophys. Res. Lett.*, *19*, 881-884, 1992.

Brandon, C., and B. Romanowicz, A "no-lid" zone in the central Chang-Thang platform of Tibet: Evidence from pure path phase velocity measurements of long-period Rayleigh waves, *J. Geophys. Res.*, *91*, 6547-6564, 1986.

Byerly, P., The dispersion of seismic waves of the Love type and the thickness of the surface layer of the Earth under the Pacific, *Beitr. Geophys.*, *26*, 27-33, 1930.

Calcagnile, G., and G. F. Panza, Crust and upper mantle structure under the Baltic Shield and Barents Sea from the dispersion of Rayleigh waves, *Tectonophysics*, *47*, 59-71, 1978.

Calcagnile, G., and G. F. Panza, Crustal and upper mantle structure beneath the Apennines region as inferred from the study of Rayleigh waves, *J. Geophys.*, *45*, 319-327, 1979.

Calcagnile, G., and G. F. Panza, Upper mantle structure of the Apulian plate from Rayleigh waves, *Pure Appl. Geophys.*, *118*, 823-830, 1980.

Calcagnile, G., and G. F. Panza, Crustal and upper mantle structure of the Mediterranean area derived from surface-wave data, *Phys. Earth Planet. Inter.*, *60*, 163-168, 1990.

Calcagnile, G., G. F. Panza, and L. Knopoff, Upper mantle structure of north-central Italy from Rayleigh waves phase velocities, *Tectonophysics*, *56*, 51-63, 1979.

Calcagnile, G., U. Mascia, V. del Gaudio, and G. F. Panza, Deep structure of southeastern Europe from the dispersion of Rayleigh waves, *Tectonophysics*, *110*, 93-111, 1985.

Cara, M., Filtering of dispersed wave trains, *Geophys. J. R. Astron. Soc.*, *33*, 65-80, 1973.

Chen, W.-P., and P. Molnar, Short-period Rayleigh wave dispersion across the Tibetan Plateau, *Bull. Seismol. Soc. Am.*, *65*, 1051-1057, 1975.

Chun, K.Y, and T. Yoshii, Crustal structure of the Tibetan Plateau: A surface wave study, *Bull. Seismol. Soc. Amer.*, *67*, 735-750, 1977.

Das, T., and G. Nolet, Crustal thickness using high frequency Rayleigh waves, *Geophys. Res. Lett.*, *22*, 539-542, 1995.

Ditmar, P.G., and T.B. Yanovskaya, A generalization of the Backus-Gilbert method for estimation of lateral variations of surface wave velocity (in Russian), *Izv. Akad. Nauk SSSR, Fiz. Zemli*, *6*, 30-60, 1987.

Dost, B., Upper mantle structure under western Europe from fundamental and higher mode surface waves using the NARS array, *Geophys. J. Int.*, *100*, 131-152, 1990.

Dziewonski, A.M., On regional differences in dispersion of mantle waves, *Geophys. J. R. Astron. Soc.*, *22*, 289-325, 1971.

Dziewonski, A. M., and D. L. Anderson, Preliminary reference Earth model, *Phys. Earth Planet. Inter.*, *25*, 297-356, 1981.

Dziewonski, A. M., S. Bloch, and M. Landisman, 1969. A technique for the analysis of transient seismic signals, *Bull. Seismol. Soc. Am.*, *59*, 427-444, 1969.

Dziewonski, A.M., T.-A. Chou, and J.H. Woodhouse, Determination of earthquake source parameters from waveform data for studies of global and regional seismicity, *J. Geophys. Res.*, *86*, 2825-2852, 1981.

Ekström, G., J. Tromp, and E.W.F. Larson, Measurements and global models of surface wave propagation, *J. Geophys. Res.*, *102*, 8137-8158, 1997.

Ewing, W.M., W.S. Jardetsky, and F. Press, *Elastic Waves in Layered Media*, McGraw-Hill, New York, 1957.

Feng, C.C., and T. Teng, Three-dimensional crust and upper mantle structure of the Eurasian continent, *J. Geophys. Res.*, *88*, 2261-2272, 1983a.

Feng, C.C., and T. Teng, An error analysis of FTAN, *Bull. Seismol. Soc. Am.*, *73*, 143-156, 1983b.

Feng, R., J.S. Zhu, Y. Y. Ding, G.Y. Chen, Z. Q. He, S. B. Yang, H. N. Zhou, and K. Z. Sun, Crustal structure in China from surface waves, *Chin. Geophys.*, Engl. Transl., *2*, 273-289, 1983.

Golitzin, B.B., On dispersion and attenuation of surface seismic waves (in Russian), *Izv. Russ. Acad. Sci.*, *2*, 1912.

Gutenberg, B., Dispersion und extinktion von seismischen oberflachenwellen und der aufbau der obersten erdschechten, *Phys. Z.*, *25*, 377-381, 1924.

Gutenberg, B., Uber gruppengeschwindigkeit bei erbebebwellen, *Phys. Z.*, *27*, 111-114, 1926.

Gutenberg, B., and C.F. Richter, On seismic waves, *Beitr. Geophys.*, *47*, 73-131, 1936.

Guterch, A., M. Grad, R. Materzak, and E. Perchuć, Deep structure of the Earth's crust in the contact zone of the Paleozoic and Precambrian Platform of Poland (TTZ), *Tectonophysics*, *128*, 251-279, 1986.

Herrin, E., and T. Goforth, Phase matched filters: application to the study of Rayleigh waves, *Bull. Seismol. Soc. Am.*, *67*, 1259, 1977.

Hill, R.I., I.H. Campbell, G.R. Davies, and R.W. Griffiths, Mantle plumes and continental tectonics, *Science*, *256*, 186-193, 1992.

Hurtig, E., G. Gräss, and R.-P. Oesburg, Velocity variation in the upper mantle beneath TE and EEP, *Tectonophysics*, *56*, 33-144, 1979.

Jeffreys, H., The effect on Love waves of heterogeneity in the lower mantle, *Mon. Not. R. Astron. Soc., Geophys. Suppl.*, *2*, 101-111, 1928.

Jeffreys, H., The surface waves of earthquakes, *Mon. Not. R. Astron. Soc., Geophys. Suppl.*, *3*, 253-261, 1935.

Jobert, N., B. Journet, G. Jobert, A. Hirn, and S.-K. Zhong, Deep structure of southern Tibet inferred from the dispersion of Rayleigh waves through a long-period seismic network, *Nature*, *313*, 386-388, 1985.

Kim, W.-Y., V. V. Kazakov, A. G. Vanchugov, and D. W. Simpson, Broadband and array observations at low noise sites in Kazakhstan: Opportunities for seismic monitoring of a Comprehensive Test Ban Treaty, *Monitoring a Comprehensive Test Ban Treaty*, edited by E. S. Husebye and A.M. Dainty, pp. 467-482, Kluwer, Norwell, Mass., 1995.

Knopoff, L., Observation and inversion of surface wave dispersion, *Tectonophysics*, *13*, 497-519, 1972.

Knopoff, L., The thickness of the lithosphere from dispersion of surface waves, *Geophys. J. R. Astron. Soc.*, *74*, 55-81, 1983.

Knopoff, L., and F.-S. Chang, Upper mantle structure under the Tibetan Plateau, in *Geological and Ecological Studies of the Qinghai-Xizang Plateau*, vol. *1*, pp. 627-632, edited by Liu D.S., Gordon and Breach, New York, 1981.

Knopoff, L., and A.A. Fouda, Upper mantle structure under the Arabian Peninsula, *Tectonophysics*, *26*, 121-134, 1975.

Knopoff, L., and F.A. Schwab, Apparent initial phase of a source of Rayleigh waves, *J. Geophys. Res.*, *73*, 755-760, 1968.

Kozhevnikov, V. M., and M. P. Barmin, Dispersion curves of Rayleigh wave group velocities for several regions of the Asian continent, in *Izv. Akad. Nauk SSSR, Fiz. Zemli*, no. 9, 16-25, 1989.

Kozhevnikov, V. M., D. E. Lokshtanov, and M. P. Barmin, Shear-velocity structure of the lithosphere for nine large tectonic regions of the Asian continent, in *Izv. Akad. Nauk SSSR, Fiz. Zemli*, no. 1, 61-70, 1992.

Krueger, F., and K. Stammler, The German Regional Seismic Network (GRSN) used as mid- and long-period array, *Eur. Geophys. Soc. Newsl.*, *58*, 57, 1996.

Kunin, N. Y., *et al.*, Basement surface relief map, Inst. of Phys. of the Earth, Acad. of Sci., Minist. of Geol. of the Russ. Fed., Moscow, 1987.

Lander, A.V., A.L. Levshin, L.I. Ratnikova, and A.N. Yakobson, Peculiarities of the deep structure of Northern Eurasia from seismic surface wave data (in Russian), *Proc. Acad. Sci. USSR*, *285 (4)*, 845-848, 1985.

Landisman, M., A. Dziewonski, and Y. Sato, Recent improvements in the analysis of surface wave observations, *Geophys. J. R. Astron. Soc.*, *17*, 369-403, 1969.

Laske, G., Global observations of off-great-circle propagation of long-period surface waves, *J. Geophys. Res.*, *90*, 605-621, 1995.

Laske, G., and G. Masters, Constraints on global phase velocity maps from long-period polarization data, *J. Geophys. Res.*, *101*, 16,059-16,075, 1996.

Lerner-Lam, A. L., and T. H. Jordan, Earth structure from fundamental and higher-mode waveform analysis, *Geophys. J. R. Astron. Soc.*, *75*, 759-797, 1983.

Lévêque, J.-J., L. Rivera, and G.W. Wittlinger, On the use of checker-board test to assess the resolution of tomographic inversions, *Geophys. J. Int.*, *115*, 313-318, 1993.

Levshin, A., and K. A. Berteussen, Anomalous propagation of surface waves in the Barents Sea as inferred from NORSAR recordings, *Geophys. J. R. Astron. Soc.*, 56, 97-118, 1979.

Levshin, A.L., and M. H. Ritzwoller, Characteristics of surface waves generated by events on and near the Chinese nuclear test site, *Geophys. J. Int.*, *123*, 131-149, 1995.

Levshin, A. L., V.F. Pisarenko, and G. A. Pogrebinsky, On a frequency-time analysis of oscillations, *Ann. Geophys.*, *28*, 211-218, 1972.

Levshin, A. L., L. Ratnikova, and J. Berger, Peculiarities of surface wave propagation across central Eurasia, *Bull. Seismol. Soc. Am.*, *82*, 2464-2493, 1992.

Levshin, A. L., M. H. Ritzwoller, and L. I. Ratnikova, The nature and cause of polarization anomalies of surface waves crossing northern and central Eurasia, *Geophys. J. Int.*, *117*, 577-590, 1994.

Levshin, A.L., M.H. Ritzwoller, and S.S. Smith, Group velocity variations across Eurasia, in *Proceedings of the 18th Seismic Research Symposium on Monitoring a CTBT*, edited by J.F. Lewkowicz, J.M. McPhetres, and D.T. Reiter, pp. 70-79, Phillips Lab., Hanscom AFB, Mass., 1996.

Levshin, A. L., T. B. Yanovskaya, A. V. Lander, B. G. Bukchin, M. P. Barmin, L. I. Ratnikova, and E. N. Its, *Seismic Surface Waves in a Laterally Inhomogeneous Earth*, edited by V. I. Keilis-Borok, Kluwer, Norwell, Mass., 1989.

Li, X.D., and B. Romanowicz, Global mantle shear velocity model developed using nonlinear asymptotic coupling theory, *J. Geophys. Res.*, *101*, 22245-22272, 1996.

Lomax, A., and R. Snieder, The contrast in the upper mantle shear-wave velocity between the East European Platform and tectonic Europe obtained with genetic algorithm inversion of Rayleigh-wave group velocity dispersion, *Geophys. J. Int.*, *123*, 169-182, 1995.

Love, A.E.H., *Some Problems in Geodynamics*, Cambridge Univ. Press, New York, 1911. (Reprinted Dover, New York, 1967.)

Lyon-Caen, H., Comparison of the upper mantle shear wave velocity structure of the Indian Shield and the Tibetan Plateau and tectonic implications, *Geophys. J. R. Astron. Soc.*, *86*, 727-749, 1986.

Makris, J., and A. Ginzburg, The Afar depression: Transition between continental rifting and sea floor spreading, *Tectonophysics*, *141*, 199-214, 1987.

Mantovani, E., G. Nolet, and G. F. Panza, Lateral heterogeneity in the crust of the Italian region from regionalized

Rayleigh-wave group velocities, *Ann. Geophys.*, *3*, 519-530, 1985.

Masters, G., S. Johnson, G. Laske, and H. Bolton, A shear-velocity model of the mantle, *Philos. Trans. R. Soc. London, Ser. A*, *354*, 1385-1411, 1996.

McNamara, D.E., T.J. Owens, and W.R. Walter, Observations of regional phase propagation across the Tibetan Plateau, *J. Geophys. Res.*, *100*, 22,215-22,229, 1995.

Mindevalli, O.Y., and B. J. Mitchell, Crustal structure and possible anisotropy in Turkey from seismic surface wave dispersion, *Geophys. J. Int.*, *98*, 93-106, 1989.

Mohr, P., Ethiopian flood basalt province, *Nature*, *303*, 577-584, 1983.

Molnar, P., P. England, and J. Martinod, Mantle dynamics, uplift of the Tibetan Plateau, and the Indian Monsoon, *Rev. Geophys.*, *31*, 357-396, 1993.

Montagner, J.P., and H.C. Nataf, A simple method for inverting the azimuthal anisotropy of surface waves, *J. Geophys. Res.*, *91*, 511-520, 1986.

Montagner, J.P., and T. Tanimoto, Global anisotropy in the upper mantle inferred from the regionalization of phase velocities, *J. Geophys. Res.*, *95*, 4794-4819, 1990.

Montagner, J.P., and T. Tanimoto, Global upper mantle tomography of seismic velocities and anisotropies, *J. Geophys. Res.*, *96*, 20337-20351, 1991.

Mooney, W.D., G. Laske, and G. Masters, CRUST 5.1: A global crustal model at 5° by 5°, *J. Geophys. Res.*, in press, 1997.

Mueller, S., and C. Sprecher, Upper mantle structure along a profile through the eastern Alps from Rayleigh wave dispersion, in *Alps, Apennines, Hellenides*, edited by H. Closs, *Int. Geodyn. Comm. Sci. Rep.*, *38*, 40-44, 1978.

Muyzert, E., and R. Snieder, The influence of errors in source parameters on phase velocity measurements of surface waves, *Bull. Seismol. Soc. Am.*, *86*, 1863-1872, 1996.

Nataf, H.-C., and Y. Ricard, 3SMAC: An a priori tomographic model of the upper mantle based on geophysical modeling, *Phys. Earth Planet. Inter.*, *95*, 101-122, 1996.

Neuenhofer, H., F. Mariller, and G. F. Panza, Crust and upper mantle structure in the Bohemian Massif from the dispersion of Rayleigh waves, *Gerlands Beitr. Geophys.*, *90*, 514-520, 1981.

Nishimura, C.E., and D.W. Forsyth, Rayleigh wave phase velocities in the Pacific with implications for azimuthal anisotropy and lateral heterogeneities, *Geophys. J. Int.*, *94*, 479-501, 1988.

Nolet, G., The upper mantle under western Europe inferred from the dispersion of Rayleigh wave modes, *J. Geophys.*, *43*, 265-276, 1977.

Nolet, G., Wave form tomography, in *Seismic Tomography with Applications in Global Seismology and Exploration Geophysics*, edited by G. Nolet, pp. 301-322, D. Reidel, Norwell, Mass., 1987.

Oliver, J., A summary of observed surface wave dispersion, *Bull. Seismol. Soc. Am.*, *52*, 81-86, 1962.

Panza, G.F., H. Neuenhofer, and G. Calcagnile, Contribution to phase velocity investigation of Rayleigh waves in middle Europe, *Pure Appl. Geophys.*, *116*, 1299-1306, 1978.

Panza, G. F., S. Mueller, and G. Calcagnile, The gross features of the lithosphere-asthenosphere system in Europe from seismic surface waves and body waves, *Pure Appl. Geophys.*, *118*, 1209-1213, 1980.

Patton, H., Crustal and upper mantle structure of the Eurasian continent from the phase velocity and Q of surface waves. *Rev. Geophys.*, *18*, 605-625, 1980.

Pavlis G., H. Al-Shukri, H. Mahdi, and D. Repin, JSP arrays and networks in Central Asia, *IRIS Newsl.*, *XIII (2)*, 10-12, 1994.

Pedersen, H. A., M. Camillo, and N. Balling, Changes in the lithospheric structure across the Sorgenfrei-Tornquist Zone inferred from dispersion of Rayleigh waves, *Earth Planet. Sci. Lett.*, *128*, 37-46, 1994.

Pines, I., T.-L. Teng, and R. Rosenthal, A surface wave dispersion study of the crustal and upper mantle structure of China, *J. Geophys. Res.*, *85*, 3829-3844, 1980.

Press, F., Determination of crustal structure from phase velocity of Rayleigh waves, I, Southern California, *Geol. Soc. Am. Bull.*, *67*, 1647-1658, 1956.

Press, F., M. Ewing, and J. Oliver, Crustal structure and surface wave dispersion in Africa, *Bull. Seismol. Soc. Am.*, *46*, 97-103, 1956.

Quinlan, D.M., Datascope: A relational database system for scientists, *Eos Trans. AGU, 75 (44)*, Fall Meet. Suppl., F431, 1994.

Ritzwoller, M.H., and E.M. Lavely, Three-dimensional seismic models of the Earth's mantle, *Rev. Geophys.*, *33*, 1-66, 1995.

Ritzwoller, M.H., A.L. Levshin, and L.I. Ratnikova, Surface wave tomography across Tibet, *Eos Trans. AGU, 77 (46)*, Fall Meet. Suppl., F675, 1996a.

Ritzwoller, M.H., A.L. Levshin, L.I. Ratnikova, and D.M. Tremblay, High resolution group velocity variations across Central Asia, in *Proceedings of the 18th Seismic Research Symposium on Monitoring a CTBT*, edited by J.F. Lewkowicz, J.M. McPhetres, and D.T. Reiter, pp. 98-107, Phillips Lab., Hanscom AFB, Mass., 1996b.

Ritzwoller, M.H., A.L. Levshin, S.S. Smith, and C.S. Lee, Making accurate continental broadband surface wave measurements, in *Proceedings of the 17th Seismic Research Symposium on Monitoring a CTBT*, edited by J.F. Lewkowicz, J.M. McPhetres, and D.T. Reiter, pp. 482-490, Phillips Lab., Hanscom AFB, Mass., 1995.

Ritzwoller, M.H., A.L. Levshin, D.M. Tremblay, and M.B. James, Broadband surface wave dispersion across the Antarctic Plate, *Eos Trans. Am. Geophys. Un.*, *77* (46), Fall Meet. Suppl., F477, 1996c.

Romanowicz, B.A., Constraints on the structure of the Tibet Plateau from pure-path phase velocities of Love and Rayleigh waves, *J. Geophys. Res.*, *87*, 6865-6883, 1982.

Romanowicz, B., M. Cara, J. F. Fels and D. Rouland, Geoscope: A French initiative in long period, three component, global seismic networks, *Eos, Trans. AGU*, *65*, 753-754, 1984.

Russell, D. W., R. B. Herrman, and H. Hwang, Application of frequency-variable filters to surface wave amplitude analysis, *Bull. Seismol. Soc. Am.*, *78*, 339-354, 1988.

Snieder, R., Large-scale waveform inversion of surface waves for lateral heterogeneity, 2, Application to surface wave in Europe and Mediterranean, *J. Geophys. Res.*, *93*, 12067-12080, 1988.

Snieder, R. Global inversions using normal modes and long-period surface waves, in *Seismic Tomography: Theory and Practice*, edited by H.M. Iyer and K. Hirahara, pp. 23-63, Chapman and Hall, New York, 1993.

Snieder, R., and H. Paulssen, Future deployment of the NARS array, in *Proceedings of the Europrobe Symposium, Jablonna 1991*, edited D.G. Gee and M. Beckholmen, pp. 129-132, C Warsawa, 1993.

Stange, S., and W. Friederich, Surface wave dispersion and upper mantle structure beneath southern Germany from joined inversion of network recorded teleseismic events, *Geophys. Res. Lett.*, *20*, 2375-2378, 1993.

Stevens, J.L., and S.M. Day, The physical basis for m_b : M_s and variable frequency magnitude methods for earthquake/explosion discrimination, *J. Geophys. Res.*, *90*, 3009-3020, 1985.

Stoneley, R., The effect of the ocean on Rayleigh waves,

Mon. Not. R. Astron. Soc., Geophys. Suppl., 1, 349-356, 1926.

Stoneley, R., Dispersion of waves in a double surficial layer, *Mon. Not. R. Astron. Soc., Geophys. Suppl., 2*, 527-531, 1928.

Su, W., R. L. Woodward, and A.M. Dziewonski, Degree 12 model of shear velocity heterogeneity in the mantle, *J. Geophys. Res., 99*, 6945-6980, 1994.

Tanimoto, T., and D. L. Anderson, Lateral heterogeneity and azimuthal anisotropy of the upper mantle: Love and Rayleigh waves 100-250 s, *J. Geophys. Res., 90*, 1842-1858, 1985.

Trampert, J., and J. Woodhouse, Global phase velocity maps of Love and Rayleigh waves between 40 and 150 seconds, *Geophys. J. Int., 122*, 675-690, 1995.

Trampert, J., and J. Woodhouse, Global azimuthal anisotropy, *Eur. Geophys. Soc. Newsl., 58*, 57, 1996.

Vaccari, F., and G. F. Panza, v_p/v_s estimation in south-western Europe from p-wave tomography and surface wave tomography analysis, *Phys. Earth Planet. Inter., 78*, 229-237, 1993.

Vdovin, O., J.A. Rial, M.H. Ritzwoller, and A.L. Levshin, Surface wave inversion of the South American lithosphere (SISAL), *Eos Trans. AGU, 77 (46)*, Fall Meet. Suppl., F464, 1996.

Vernon, F., The Kyrghyz Seismic Network, *IRIS Newsl., 13*, 7-8, 1994.

Vernon, F., Mellors, R.J., J. Berger, A.M. Al-Amri, and J. Zollweg, Initial results from the deployment of broadband seismometers in the Saudi Arabian Shield, in *Proceedings of the 18th Seismic Research Symposium on Monitoring a CTBT*, edited by J.F. Lewkowicz, J.M. McPhetres, and D.T. Reiter, pp. 108-117, Phillips Lab., Hanscom AFB, Mass., 1996.

Wessel, P., and W.H. F. Smith, Free software helps map and display data, *Eos Trans. AGU, 72*, 441, 1991.

Wessel, P., and W.H. F. Smith, New version of the Generic Mapping Tools released, *Eos Trans. AGU, 76*, 329, 1995.

White, R., and D. McKenzie, Magmatism at rift zones: The generation of volcanic continental margins and flood basalts, *J. Geophys. Res., 94*, 7685-7729, 1989.

Wier, S., Surface wave dispersion and Earth structure in south-eastern China, *Geophys. J. R. Astron. Soc., 69*, 33-47, 1982.

Wu, F.T., and A. Levshin, Surface wave group velocity tomography of East Asia, *Phys. Earth Planet. Inter., 84*, 59-77, 1994.

Wu, F.T., A.L. Levshin, and V.M. Kozhevnikov, Rayleigh wave group velocity tomography of Siberia, China, and the vicinity, *Pure Appl. Geophys., 149*, 447-473, 1997.

Yanovskaya, T.B., and P.G. Ditmar, Smoothness criteria in surface wave tomography, *Geophys. J. Int., 102*, 63-72, 1990.

Yanovskaya, T. B., G. F. Panza, P. G. Ditmar, P. Suhadolc, and S. Mueller, Structural heterogeneity and anisotropy based on 2-D phase velocity patterns of Rayleigh waves in western Europe, *Atti Acad. Naz. Lincei, 1*, 127-135, 1990.

Zeng, Y., T.-L. Teng, and K. Aki, Surface wave mapping of the crust and upper mantle in the Arctic Region, *Bull. Seismol. Soc. Am., 79*, 1520-1541, 1989.

Zhang, Y.-S., Three-dimensional velocity structure beneath East Asia and its tectonic implication, *Mantle Dynamics and Plate Interactions in East Asia, Geophys. Monogr. Ser.*, edited by M.F.J. Flower and S.-L. Chung, AGU, Washington, D.C., in press, 1997.

Zhang, Y.-S., and T. Tanimoto, High resolution global upper mantle structure and plate tectonics, *J. Geophys. Res., 98*, 9793-9823, 1993.

Zhao, L.-S., and J. Xie, Lateral variations in compressional velocities beneath the Tibetan Plateau from P_n traveltime tomography, *Geophys. J. Int., 115*, 1070-1084, 1993.

Zielhuis, A., and G. Nolet, Shear velocity variations in the upper mantle beneath central Europe, *Geophys. J. Int., 117*, 695-715, 1994.

Zonenshain, L. P., M. I. Kuzmin, and L. M. Natapov, *Geology of the USSR: A Plate-Tectonic Synthesis, Geodyn. Ser.*, vol. 21, edited by B. M. Page, AGU, Washington, D. C., 1990.

A.L. Levshin and M.H. Ritzwoller, Department of Physics, University of Colorado, Campus Box 390, Boulder, CO, 80309-0390. (e-mail: levshin@lemond.colorado.edu; ritzwoller@lemond.colorado.edu)

(Received April 1, 1997; revised September 10, 1997; accepted September 12, 1997.)